Diffusion in Multi-Component Liquids: from Microscopic to Macroscopic Scales

G. Guevara-Carrion,[†] Y. Gaponenko,[‡] T. Janzen,[†] J. Vrabec,[†] and V. Shevtsova[*,‡]

[†]*Thermodynamics and Energy Technology, University of Paderborn, 33098 Paderborn, Germany*

[‡]*Microgravity Research Center, Université Libre de Bruxelles (ULB), CP–165/62, Av. F.D. Roosevelt, 50, B–1050 Brussels, Belgium*

E-mail: vshev@ulb.ac.be

Phone: +32 2 650 65 70

Abstract

In spite of considerable research on the nature of aqueous alcohol mixtures that are characterized by microscopic inhomogeneity or incomplete mixing at the molecular level, transport properties have received little attention. We report the results of a study on diffusion in the ternary mixture of water with two alcohols, *i.e.*, water + methanol + ethanol, which is investigated on microscopic and macroscopic scales by means of molecular simulation and Taylor dispersion experiments. A novel protocol is developed for the comparison of mutual diffusion coefficients sampled by two fundamentally different approaches, which allows for their critical analysis. Because of complex intermolecular interactions, given by the presence of hydrogen-bonding, the analysis of transport processes in this mixture is challenging for not only on the microscopic scale for simulation techniques but also on the macroscopic scale due to unfavorable optical properties. Binary limits of the Fick diffusion matrix are used for validation of the experimental ternary mixture results together with the verification of the validity of the phenomenological Onsager reciprocal relations. The Maxwell-Stefan diffusion coefficients and the thermodynamic factor are sampled by molecular simulation consistently on the basis of given force field models. The protocol for the comparison of the results from both approaches is also challenging because Fick diffusion coefficients of ternary mixtures depend on the frame of reference. Accordingly, the measured coefficients are transformed from the volume-averaged to the molar-averaged frame of reference and it is demonstrated that both approaches provide not only similar qualitative behavior along two concentration paths but also strong quantitative agreement. This coordinated work using different approaches to study diffusion in multi-component mixtures is expected to be a significant step forward for the accurate assessment of cross diffusion.

Introduction

Mixtures of alcohol and water are particularly complex systems that are challenging from the point of view of both simulation and experiment. In spite of considerable research into the nature of alcohol-water mixtures at the molecular level there still seem to be few studies on their macroscopic

properties, particularly for ternary mixtures. Water and methanol are the two most prominent hydrogen-bonding liquids and their mixture has consequently been the subject of many studies. Thorough research was undertaken for the methanol-water mixture concerning the influence of segregation, clustering and the resulting molecular structures mainly in the water-rich and water-poor concentration ranges[1–3].

Binary data on the Fick diffusion coefficient are relatively abundant, in fact, both tracer and mutual diffusion coefficients of all binary subsystems of the present ternary mixture were measured over the full composition range[4–6]. However, the presence of coupled diffusion makes mutual diffusion measurements in ternary systems more complicated because four Fick diffusion coefficients have to be determined from a signal for two components. Indeed, the first experimental verification of the existence of cross diffusion was reported a hundred years later[7] than experimental and theoretical investigations of binary liquid mixtures[8].

Analyses of diffusion problems are typically based on the assumption of a binary system, *i.e.*, either the mixture actually contains only two components, or, for dilute multicomponent systems, only binary pairs are considered. However, in general, the concentration profiles cannot be accurately modeled by means of binary analysis, and multicomponent diffusion equations are a necessity[9]. Hence, there is great interest in the improvement of experimental methodologies and in the development of reliable methods for the prediction of mutual diffusion coefficients of mixtures containing three or more components.

Owing to the rapid development of computing power, molecular modelling and simulation has emerged as a powerful tool to complement experimental efforts[10]. Force field-based simulation methods can contribute to the understanding and interpretation of experimental results, to obtain predictive estimates and to inter- or extrapolate experimental data into regions that are difficult to access in the laboratory[11]. Experimentally, the Fick diffusion coefficient can be measured on the basis of a variety of techniques from optical interferometry to NMR spin relaxation. In the present work, Taylor dispersion, also known as peak broadening technique, was employed.

Molecular simulation studies on diffusion coefficients of complex liquid mixtures containing

three or more components are almost absent. Liu et al.[12] consistently predicted the Fick diffusion coefficients of the ternary mixture chloroform + acetone + methanol, however, they were not able to verify their results due to the lack of experimental data. The ternary mixture water + methanol + ethanol was also studied by Liu et al.[13] by means of equilibrium molecular dynamics (EMD) simulation, but solely in the region of infinite dilution. In most cases EMD has been employed to predict the dynamic properties of aqueous solutions of methanol[14–17] or ethanol[14,17–20].

To the best of our knowledge, the diffusivity of the ternary mixture water + methanol + ethanol has not been studied by experiment before. In a preceding work[6] on that ternary mixture, the mutual diffusion coefficients of all binary subsystems were predicted in a consistent manner, *i.e.*, the Maxwell-Stefan diffusion coefficients and the thermodynamic factor matrix were obtained by means of molecular simulation. Pronounced minima of the mutual diffusion composition dependence for the strongly non-ideal binary subsystems water + methanol and water + ethanol were accurately predicted. For the ternary mixture water + methanol + ethanol, a few data points were predicted as well, but could not be assessed on the basis of experimental data at that time. One of the aims of this work is to complement that effort, comparing simulations with experiments over the whole composition range.

This study is the first to combine molecular simulation and experiment to determine diffusion coefficients of a ternary mixture comprising water and two alcohols with low molar mass, *i.e.*, water + methanol + ethanol. The paper is organized as follows. First, a brief explanation of the general equations governing diffusive fluxes in ternary mixtures is given. Second, the experimental methodology is described in detail, followed by a brief outline of the employed simulation techniques. Subsequently, the experimental and simulation results for the Fick diffusion coefficient matrix are presented, analyzed and compared with each other. The predicted intra-diffusion coefficients are also studied in the light of the microscopic structure of the mixture. Finally, conclusions are drawn.

General description of diffusion

Fick's law is the most common approach to describe mass transport in liquid mixtures. It relates a mass flux to a gradient of its driving force[21]. When the driving force is expressed in terms of the gradient of molar concentration ∇C_j, the diffusive molar flux of component i in the volume-averaged frame of reference J_i^V for a mixture containing N components is written as

$$J_i^V = -\sum_{j=1}^{N-1} D_{ij}^V \nabla C_j\,, \quad (i = 1,\ldots,N-1)\,. \tag{1}$$

If the driving force is expressed in terms of the gradient of mole fraction ∇x_j, the diffusive molar flux J_i^M in the molar-averaged frame of reference is

$$J_i^M = -\rho^M \sum_{j=1}^{N-1} D_{ij}^M \nabla x_j\,, \quad (i = 1,\ldots,N-1)\,, \tag{2}$$

where ρ^M is the molar density of the mixture. Because the molar fluxes depend on the choice of a frame of reference, the diffusion coefficients are defined accordingly. The Fick diffusion coefficients in the volume- and molar-averaged frames of reference are denoted by D_{ij}^V and D_{ij}^M, respectively.

The Fick approach involves $N-1$ independent diffusion fluxes and a $(N-1)\times(N-1)$ matrix of diffusion coefficients, which is generally not symmetric, *i.e.*, $D_{ij} \neq D_{ji}$. The main diffusion coefficients D_{ii} connect the flux of component i to its own concentration gradient, while the cross diffusion coefficients D_{ij} describe the coupled flux of component i induced by the concentration gradient of component j[22]. Numerical values of D_{ij} depend both on the frame of reference for velocity (molar-, mass- or volume-averaged) and on the order of the components.

In the present simulations the molar-averaged frame of reference was used to obtain the Fick diffusion coefficients, where the following holds

$$\sum_{i=1}^{N} J_i^M = 0\,. \tag{3}$$

On the other hand, the mathematical model of the Taylor dispersion technique in ternary mixtures was originally developed for the volume-averaged frame of reference[23]. Here, the sum of fluxes is defined as

$$\sum_{i=1}^{N} J_i^V v_i = 0\,, \tag{4}$$

where v_i is the partial molar volume of component i in the mixture.

The diffusion coefficient matrix in the volume-averaged frame of reference $\mathbf{D}^V$ obtained experimentally from the Taylor dispersion technique can be transformed into its form in the molar-averaged frame of reference $\mathbf{D}^M$ in order to be compared with the diffusion coefficient matrix obtained from EMD by[21]

$$[\mathbf{D}^M] = [\mathbf{B}^{uV}][\mathbf{D}^V][\mathbf{B}^{Vu}], \tag{5}$$

where the elements of the matrices are given by

$$\begin{aligned} B_{ik}^{Vu} &= \delta_{ik} - x_i\left(v_k - v_N\right)/v, \\ B_{ik}^{uV} &= \delta_{ik} - x_i\left(1 - v_k/v_N\right), \end{aligned} \tag{6}$$

δ_{ij} stands for the Kronecker delta function and

$$v = \sum_{i=1}^{N} x_i v_i. \tag{7}$$

The required partial molar volume v_i can be calculated straightforwardly from the partial molar excess volume v_i^{E} given by[24]

$$v_i^{\mathrm{E}} = v^{\mathrm{E}} - \sum_{k\neq i}^{N} x_k \left(\frac{\partial v^{\mathrm{E}}}{\partial x_k}\right)_{T,p,x_{j\neq i,k}}, \tag{8}$$

which was done here on the basis of experimental literature data[25].

There are two approaches for the selection of the component order: one is based on the molar mass and the other one on the density of the components in their pure state. In EMD the use of molar mass is appropriate and the components with a higher (or lower) molar mass are typically chosen as the independent ones. Hydrodynamic effects become important when liquid mixtures are studied on a macroscopic scale. Thus, for experimental work, it is appropriate to choose the components with the higher density in their pure state as the independent ones. Following the latter convention, water and methanol were chosen as the independent components for the present analysis of water (1) + methanol (2) + ethanol (3). This order corresponds to increasing molar mass, cf. Table 1.

Diffusion in multicomponent mixtures can also be described by Maxwell-Stefan (MS) theory. Here, the driving force is expressed in terms of the gradient of the chemical potential $\nabla\mu_i$, which is assumed to be balanced by a friction force that is proportional to the mutual velocity $\mathbf{u}_i - \mathbf{u}_j$ between the components[21]

$$\sum_{j\neq i=1}^{N} \frac{x_j(\mathbf{u}_i - \mathbf{u}_j)}{Đ_{ij}} = -\beta\nabla\mu_i\,, \tag{9}$$

where $\beta = 1/(k_\mathrm{B}T)$ is the Boltzmann factor. The MS diffusion coefficient $Đ_{ij}$ thus plays the role of an inverse friction coefficient between components i and j. MS diffusivities are symmetric, *i.e.*, $Đ_{ij} = Đ_{ji}$, so that there are only $N(N-1)/2$ independent MS diffusion coefficients.

Because Fick's law and MS theory describe the same phenomenon, a relation between both sets of diffusion coefficients exists[21]

$$\mathbf{D}^M = \mathbf{B}^{-1}\boldsymbol{\Gamma}\,, \tag{10}$$

in which all three symbols represent $(N-1)\times(N-1)$ matrices. $\mathbf{D}^M$ is the matrix of Fick diffusion coefficients in the molar-averaged frame of reference D_{ij}^M, where the elements of the matrix $\mathbf{B}$ are defined by[26]

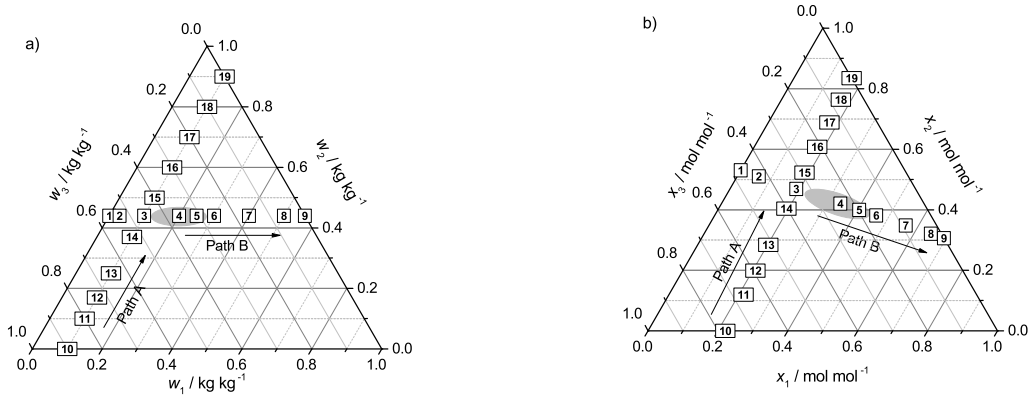

Figure 1: Concentration matrices in mass (a) and mole (b) fractions for the mixture water (1) + methanol (2) + ethanol (3). The squares represent the state points for which Fick diffusion coefficients were measured, indicating their running number. Poor optical properties were encountered in the shaded composition range.

$$B_{ii} = \frac{x_i}{Đ_{iN}} + \sum_{j\neq i=1}^{N} \frac{x_j}{Đ_{ij}}, \qquad B_{ij} = -x_i \left(\frac{1}{Đ_{ij}} - \frac{1}{Đ_{iN}} \right), \tag{11}$$

and the matrix of the thermodynamic factor $\mathbf{\Gamma}$ is given by

$$\Gamma_{ij} = \delta_{ij} + x_i \frac{\partial \ln \gamma_i}{\partial x_j}\bigg|_{T,p,x_{k,k\neq j=1\ldots N-1}}, \tag{12}$$

where γ_i stands for the activity coefficient of component i. In this way, the MS diffusion coefficients can be transformed to the Fick diffusion coefficients and vice versa, if the thermodynamic factor matrix is known.

The MS approach separates mass transfer dynamics from thermodynamics, which is considered by the thermodynamic factor. The MS diffusion coefficients are related to chemical potential gradients and therefore cannot directly be measured in the laboratory. However, they can well be sampled by EMD employing the Green-Kubo formalism or, alternatively, from the mean square displacement. $\mathbf{\Gamma}$ serves as a conversion factor between Fick and MS diffusion coefficients, therefore, its knowledge is necessary to determine Fick diffusion coefficient data on the basis of EMD.

The thermodynamic factor is usually estimated from experimental vapor-liquid equilibrium (VLE) or excess enthalpy data[27,28], employing an equation of state or an excess Gibbs energy G^{E}

model, such as Margules, Wilson, NRTL or UNIQUAC. However, the resulting thermodynamic factor may be a major source of uncertainty. *I.e.*, it highly depends on the underlying thermodynamic model[28] and it corresponds only to the thermodynamic conditions under which VLE data were measured. In recent years, there has been a growing effort to sample the thermodynamic factor directly by molecular simulation, *e.g.*, based on Kirkwood-Buff theory[29–31] or free energy perturbation methods to obtain the composition dependence of the chemical potential[6,32,33]. In this work, the thermodynamic factor was calculated from the composition dependence of the chemical potential at constant temperature and pressure by Monte Carlo (MC) simulation as described in preceding work[6].

Particle-based EMD simulations are typically conducted by specifying mole fractions x_i. In experiments it is preferred to deal with directly accessible concentration variables, *i.e.*, mass fractions w_i. Previously it has been shown [34] that a transformation of the governing equations of the Taylor dispersion technique, originally written in terms of molar concentration C_i, to mass fraction w_i does not change their functional form. Consequently, both mass and mole fraction units can be found in this study. The connection between them and the molar concentration is given by

$$w_i = x_i M_i/M, \quad w_i = C_i M_i/\rho, \quad x_i = C_i M/\rho\,, \tag{13}$$

where M_i is the molar mass of component i, M is the average molar mass of the mixture and ρ is the mass density of the mixture.

Table 1: Pure component properties at 298.15 K and 0.1 MPa: molar mass M/ g mol^{-1}, mass density ρ/ kg m^{-3} and refractive index n at wavelengths λ=670 nm and 935 nm.

	water	methanol	ethanol
ρ	1000	792	789
M	18.02	32.04	46.07
$n_{\lambda=670\,\mathrm{nm}}$	1.32893	1.32447	1.35635
$n_{\lambda=935\,\mathrm{nm}}$	1.32383	1.32039	1.35236

Onsager reciprocal relations

Diffusion in multicomponent mixtures can also be described on the basis of irreversible thermodynamics. Here, the Onsager matrix $\mathbf{H}$, that relates the molar diffusive fluxes to the chemical potential gradients, is defined. This formulation is equivalent to Fick and MS postulates so that[21]

$$\mathbf{B}^{-1}\boldsymbol{\Gamma} = \mathbf{D}^{M} = \mathbf{H}^{-1}\mathbf{G}, \tag{14}$$

where the elements of the symmetric Hessian matrix $\mathbf{G}$ are given by[21]

$$G_{ij} = \frac{\partial(\mu_j - \mu_N)}{\partial x_i} = G_{ji}. \tag{15}$$

The matrix $\mathbf{G}$ can be obtained similarly as the thermodynamic factor matrix $\boldsymbol{\Gamma}$ employing an equation of state or a G^{E} model. Further, following the second postulate of irreversible thermodynamics, the phenomenological Onsager matrix $\mathbf{H}$ is also symmetric, *i.e*, $\mathbf{H} = \mathbf{H}^{\mathrm{T}}$, which expresses the Onsager reciprocal relations[21].

The symmetry property of the matrices $\mathbf{G}$ and $\mathbf{H}$ restricts the values of the Fick diffusion matrix $\mathbf{D}^{M}$. For a ternary mixture, Eq. (14) leads to a single relationship[35]

$$-G_{11}D_{12}^{M} + G_{12}D_{11}^{M} = -G_{22}D_{21}^{M} + G_{21}D_{22}^{M}, \tag{16}$$

so that there are only three independent Fick diffusion coefficients D_{ij}[21]. Therefore, the restriction given by Eq. (16) can be used as a consistency test for measured data[35]. For this purpose, a simple method to evaluate the difference between both sides of Eq. (16), and therefore the degree of asymmetry of the matrix $\mathbf{D}^{M}\mathbf{G}^{-1}$, has been proposed in the literature[36]

$$\delta_{\mathrm{Ons}}(\%) = 100\% \frac{2(F_1 - F_2)}{(F_1 + F_2)}, \tag{17}$$

where F_1 and F_2 correspond to the left and right hand sides of Eq. (16), respectively. δ_{Ons} was obtained here with the Fick diffusion coefficients in the molar-averaged frame of reference. The

matrix **G** was calculated employing the Wilson G^{E} model fitted to experimental VLE data.

Ternary diffusion coefficients approaching binary limits

In this study, we had the unique opportunity to compare measured and simulated diffusion coefficients, nevertheless, for ternary mixtures an independent control of measurements is a necessity. The behavior of ternary diffusion coefficients when approaching the binary limits provides an efficient way for the validation of the experimental and simulation results. The asymptotic behavior was previously developed for a mixture with vanishing excess volume, *i.e.*, 1,2,3,4-tetrahydronaphthaline (THN) + isobutylbenzene (IBB) + *n*-dodecane (C12)[37], when the fluxes can be written in a similar form in the volume-averaged and mass-averaged frames of reference. Here we present a complete analysis of the asymptotic behavior of diffusion coefficients measured by Taylor dispersion.

The two independent diffusive fluxes in the volume-averaged frame of reference (cf. Eq. (1)) can be written using mass fractions as

$$-J_1^V/\rho = \frac{1}{M_1} D_{11}^V \nabla w_1 + \frac{1}{M_2} D_{12}^V \nabla w_2\,, \tag{18}$$

$$-J_2^V/\rho = \frac{1}{M_1} D_{21}^V \nabla w_1 + \frac{1}{M_2} D_{22}^V \nabla w_2. \tag{19}$$

When approaching the binary mixture at the bottom of the triangle in Fig. 1a, the content of w_2 tends to zero as well as its mass flux, *i.e.*, $\nabla w_2 \to 0$ and $J_2^V \to 0$. Then, from Eq. (19) it follows that $D_{21} \to 0$, and from Eq. (18) it follows that $D_{11} \to D_{bin}^{w_1-w_3}$.

A similar analysis on the left hand side of the triangle, *i.e.*, $w_1 \to 0$ provides that $D_{12} \to 0$ and $D_{22} \to D_{bin}^{w_2-w_3}$. The behavior of the other diffusion coefficients cannot be predicted from this analysis. Note that the asymptotic behavior in the limits $w_1 \to 0$ and $w_2 \to 0$ does not depend on the frame of reference and coincides with the one reported previously[37]. However, the asymptotic behavior on the right hand side of the triangle *does* depend on the frame of reference.

Following Fick's law, the diffusive flux of the third component J_3^V can be written as

$$J_3^V = -(J_1^V v_1 + J_2^V v_2)/v_3 = \\ \frac{\rho}{v_3}\left[\frac{1}{M_1}\left(v_1 D_{11}^V + v_2 D_{21}^V\right)\nabla w_1 + \frac{1}{M_2}\left(v_1 D_{12}^V + v_2 D_{22}^V\right)\nabla w_2\right]. \quad (20)$$

Selecting the mass fractions of the second and third components as independent variables, it follows from the condition $w_1 + w_2 + w_3 = 1$ that $\nabla w_1 = -\nabla w_2 - \nabla w_3$ and the expressions for the diffusive fluxes J_2^V and J_3^V take the form

$$J_2^V = -\rho\left[\left(\frac{1}{M_2}D_{22}^V - \frac{1}{M_1}D_{21}^V\right)\nabla w_2 - \frac{1}{M_1}D_{21}^V \nabla w_3\right], \quad (21)$$

$$J_3^V = \frac{\rho}{v_3}\left\{-\left[\frac{1}{M_1}\left(v_1 D_{11}^V + v_2 D_{21}^V\right) - \frac{1}{M_2}\left(v_1 D_{12}^V + v_2 D_{22}^V\right)\right]\nabla w_2\right\} \\ -\frac{\rho}{v_3}\left[\frac{1}{M_1}\left(v_1 D_{11}^V + v_2 D_{21}^V\right)\nabla w_3\right]. \quad (22)$$

Applying the same logic as above, from the conditions $w_3 \to 0$ and $J_3^V \to 0$ it follows that

$$D_{22}^V - \frac{M_2}{M_1}D_{21}^V = D_{bin}^{w_1 - w_2}, \quad (23)$$

and

$$\frac{1}{M_1}\left(v_1 D_{11}^V + v_2 D_{21}^V\right) - \frac{1}{M_2}\left(v_1 D_{12}^V + v_2 D_{22}^V\right) = 0. \quad (24)$$

Indeed, the results from Ref.[37] for the ideal mixture with equal molar masses are reproduced.

Experiments by Taylor dispersion

The Taylor dispersion technique is based on the diffusive spreading of a small volume of a solution injected into a laminar stream of the same mixture with a slightly different composition. As the injected concentration pulse is carried through a tube, it is deformed by the coupled action of convection in axial direction and diffusion in radial direction. At the end of the capillary, a refrac-

tive index detector monitors the concentration of the eluted peak (also known as Taylor peak) as a function of time. The Fick diffusion coefficients are calculated from the resulting profile of the refractive index variation.

A detailed description of the experimental set-up used in this study was published previously[34,35,37], here only some practical information is provided. The inner diameter and length of the polytetrafluoroethylene tube were $2R_0 = 748 \pm 1\,\mu$m and $L = 29.839 \pm 0.001$ m, respectively. The capillary was coiled around a grooved aluminum cylinder with a diameter of 30 cm and was placed together with a refractometer and a pump in a temperature-regulated air bath at 298±0.2 K. The flow rate was 0.08 mL/min and the injected volume was ΔV = 20 μL.

The following substances were used without further purification: water pure from Acros Organics, deionized reagent Grade 3 (CAS Number: 7732-18-5), methanol of analytical reagent grade from Fisher Scientific (CAS Number: 67-56-1) and ethanol absolute of analytical reagent grade from VWR (CAS Number: 64-17-5).

The concentrations C_1 and C_2 at the end of the diffusion tube are given by the fundamental working equations of Price[23]

$$C_i(t) - C_i^0 = \frac{2\Delta V}{R^3 U_0}\sqrt{\frac{3}{\pi^3 t}}\Big(A_{i1}\sqrt{\hat{D}_1}\exp(-\hat{D}_1\eta) + A_{i2}\sqrt{\hat{D}_2}\exp(-\hat{D}_2\eta)\Big)\,, \quad i = 1,2\,, \tag{25}$$

where η stands for $12(t-t_R)^2/R^2t$, C_i^0 is the molar concentration of component i in the carrier liquid and ΔV is the volume of the injected solution sample. The eigenvalues $\hat{D}_i$ of the Fick diffusion matrix D_{ij} are given by

$$\hat{D}_1 = \frac{D_{11} + D_{22} + \sqrt{(D_{11}-D_{22})^2 + 4D_{12}D_{21}}}{2}\,, \tag{26}$$

$$\hat{D}_2 = \frac{D_{11} + D_{22} - \sqrt{(D_{11}-D_{22})^2 + 4D_{12}D_{21}}}{2}\,, \tag{27}$$

and the coefficients A_{ik} are defined as

$$A_{11} = \frac{(D_{22}^V - \hat{D}_1)\Delta C_1 - D_{12}^V \Delta C_2}{\hat{D}_2 - \hat{D}_1}, \tag{28}$$

$$A_{12} = \frac{(D_{22}^V - \hat{D}_2)\Delta C_1 - D_{12}^V \Delta C_2}{-(\hat{D}_2 - \hat{D}_1)}, \tag{29}$$

$$A_{21} = \frac{(D_{11}^V - \hat{D}_1)\Delta C_2 - D_{21}^V \Delta C_1}{\hat{D}_2 - \hat{D}_1}, \tag{30}$$

$$A_{22} = \frac{(D_{11}^V - \hat{D}_2)\Delta C_2 - D_{21}^V \Delta C_1}{-(\hat{D}_2 - \hat{D}_1)}, \tag{31}$$

where $A_{11} + A_{12} = \Delta C_1$ and $A_{21} + A_{22} = \Delta C_2$. Here $\Delta C_i = (C_i - C_i^0)$ is the concentration difference between injected sample and carrier liquid. Superscript V indicates that the measured Fick diffusion coefficients correspond to the volume-averaged frame of reference. The eigenvalues do not depend on the frame of reference and, correspondingly, there are no superscripts in Eqs. (26) and (27).

The determination of four Fick diffusion coefficients D_{ij}^V experimentally by fitting is a notoriously difficult problem. One important issue is the selection of a proper initial guess. A promising idea is to measure diffusion coefficients of ternary mixtures along a concentration path, starting with a binary subsystem and moving towards another one. This creates a positive feedback loop: the initial guess can be taken from a preceding state point, which, in turn, can be checked by the continuity of the diffusion coefficient data. Measurements of single state points may lead to fitting problems and even to an inversion of the numerical values of the main elements of the diffusion matrix[37–39]. Fig. 1 presents the chosen paths in terms of mass and mole fractions: path A corresponds to a constant mass fraction of water (w_1=0.1 kg kg^{-1}) and path B corresponds to a constant mass fraction of methanol (w_2=0.44 kg kg^{-1}).

Optical properties of the mixture

The refractive index detector provides an electrical voltage signal $V(t)$ which is assumed to be linearly proportional to small concentration changes of all components of the mixture[40]

$$V(t) = \sum_{i=0}^{m} \zeta_i t^i + [R_1(w_1(t) - w_1^0)] + [R_2(w_2(t) - w_2^0)], \tag{32}$$

where $R_i = \partial V/\partial w_i$ is the sensitivity of the detector to component i. This linear dependence assumes small concentration differences Δw_i between injected sample and carrier liquid. The first term in Eq. (32) compensates the drift of the detector baseline which was modeled by a polynomial fit of order m, usually m=2.

The sensitivity R_i depends on the optical properties of the mixture, *i.e.*, on the variation of the refractive index with concentration $\partial n/\partial C_i$ (contrast factor) at the wavelength of the detector

$$R_i = \partial V/\partial w_i = (\partial V/\partial n)(\partial n/\partial w_i), \tag{33}$$

where $(\partial V/\partial n)$ is a constant of the detector. The ratio of contrast factors, the so called sensitivity ratio S_R, contributes substantially to the accuracy of Taylor measurements for a given system

$$S_R = \left(\frac{\partial n}{\partial w_1}\right)_{w_2} / \left(\frac{\partial n}{\partial w_2}\right)_{w_1}. \tag{34}$$

Note that the optical sensitivity depends on the concentration units[34], *i.e.*, $S_R(C) = S_R(w)M_1/M_2$.

We were aware of the difficulties using the Taylor dispersion technique for systems containing water and methanol from a study on water + methanol + acetone due to unfavorable relative detector sensitivity[41]. Keeping this in mind, two different approaches for the accurate determination of contrast factors were used: measuring the refractive index at the wavelength of the detector as well as calculating it from the peak area and the injected amount. Taylor peaks were detected by a Knauer Smartline RI Detector 2300 which operates at the wavelength λ = 950 nm. Literature data for the contrast factors at wavelengths $\lambda > 900$ nm are available only for a limited number

of ternary mixtures[42–44]. Thus, the refractive index at the nearest available wavelength λ=935 nm and, for reference, at λ=670 nm was measured.

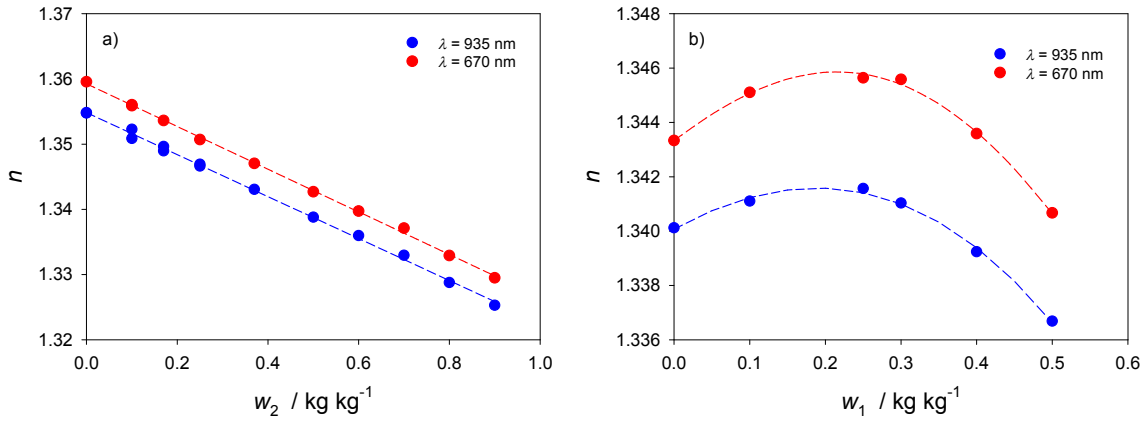

Figure 2: Measured refractive index of the mixture water (1) + methanol (2) + ethanol (3) as a function of mass fraction at different wavelengths for a constant mass fraction of water $w_1 = 0.1$ kg kg^{-1} (path A) and $w_2 = 0.44$ kg kg^{-1} (path B). Note the difference in the vertical scales.

The measured refractive index along paths A and B is listed in Table 2 and presented in Fig. 2. Along path A the curves $n(w_2)$ at different wavelengths reveal nearly parallel lines over the entire concentration space and, as expected, with the increase of λ the refractive index decreases. The measured data $n(w_2)$ along path A were interpolated by a linear function as seen in Fig. 2a, and the contrast factors are $(\partial n/\partial w_2)_{w_1,\lambda=935\,\mathrm{nm}}$ = -0.0322 and $(\partial n/\partial w_2)_{w_1,\lambda=670\,\mathrm{nm}}$ = -0.0328. For validation of the measurements, the values of n at the binary limits in the case of λ=670 nm were favorably compared with literature data.

Fig. 2b presents the variation of the refractive index along path B. The much weaker dependence of $n(w_1)$ at both wavelengths has a similar shape, displaying a maximum. The measured $n(w_1)$ data were interpolated by a suitable function and its differentiation provided the contrast factor $(\partial n/\partial w_1)_{w_2}$ which decreases with concentration w_1 at both wavelengths. In particular, this derivative changes its sign in the vicinity of state point #4, which occurs at w_1=0.179 kg kg^{-1} for λ=935 nm and w_1=0.215 kg kg^{-1} for λ=670 nm. This region with poor optical properties along path B is shaded in Fig. 1a. Moving to the apex of the composition triangle, the location of the vanishing derivative is shifted to smaller concentrations of water. Finally, the sensitivity ratio S_R

Table 2: Measured refractive index of the mixture water (1) + methanol (2) + ethanol (3) at two different wavelengths λ for a constant mass fraction of water $w_1 = 0.1$ kg kg^{-1} (path A) and $w_2 = 0.44$ kg kg^{-1} (path B).

Path A			
Point #	w_2	$n_{\lambda=670\,\mathrm{nm}}$	$n_{\lambda=935\,\mathrm{nm}}$
10	0	1.35956	1.35480
11	0.1	1.35597	1.35158
12	0.17	1.35362	1.34931
13	0.25	1.35070	1.34678
14	0.37	1.34704	1.34307
15	0.5	1.34270	1.33879
16	0.6	1.33972	1.33597
17	0.7	1.33711	1.33295
18	0.8	1.33291	1.32877
19	0.9	1.32949	1.32529
Path B			
Point #	w_1	$n_{\lambda=670\,\mathrm{nm}}$	$n_{\lambda=935\,\mathrm{nm}}$
1	0	1.3433	1.3401
3	0.1	1.3451	1.3411
5	0.25	1.3456	1.3416
6	0.3	1.3456	1.3410
7	0.4	1.3436	1.3392
8	0.5	1.3407	1.3367

was used as a fitting parameter in a small region around the originally measured values.

Selection of injected samples

We have experience in subtracting data from the measured peaks in ternary mixtures[34,35,37]. However, for the present mixture we faced a severe problem with the fitting procedure for some state points along both paths. Rather often the solution converged to a set of diffusion coefficients which did not correspond to the asymptotic predictions[37]. In this section we discuss the handling of the region with poor optical properties using a diverse selection of injected samples.

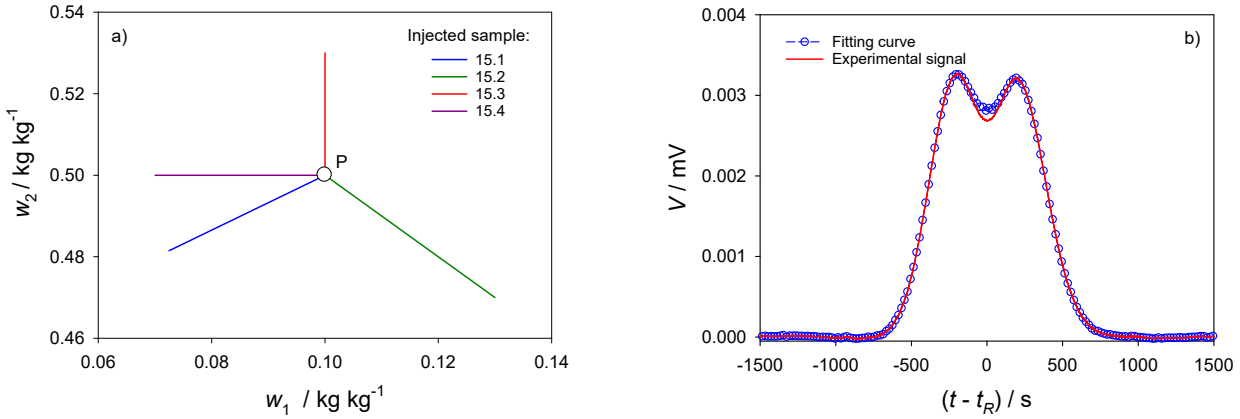

Figure 3: (a) Diffusion couples, *i.e.*, concentration of the carrier liquid (point P) and injected samples used in the experiments measuring diffusion coefficients at state point #15 of the mixture water (1) + methanol (2) + ethanol (3); (b) Ternary dispersion profile and fitting curve in the ternary mixture with injected sample 15.1.

The typical protocol for the selection of injections is the following: a first sample is injected with $\Delta w_1 = 0$, a second one with $\Delta w_2 = 0$ and a complimentary one where both mass fractions are non-zero. From Eq. (32) it follows that due to the smallness of the derivative, *i.e.*, R_1, the net variation of the refractive index Δn can be very low for the injection with Δw_2=0. Thus, we rely on the injections with non-zero diffusion couples, *i.e.*, when $\Delta w_1 \neq 0$ and $\Delta w_2 \neq 0$ simultaneously. Schematically, the considered injected samples for state point #15 are presented in Fig. 3a. Non-perpendicular injections very often lead to a peak with dips as shown in Fig. 3b. Our code can treat such peaks satisfactorily. *E.g.*, a stable solution for state point #15 was obtained using simultaneous fitting of the four peaks obtained with injections 15.2 and 15.4; all of them were repeated

twice. Each peak was initially treated as a binary mixture and pseudo-diffusion coefficients were determined. The peak quality was controlled by the reproducibility of the pseudo-diffusion coefficients. For this purpose, the experiment with the same injection was repeated up to four times. The number of injected samples varied between four and six, depending on fitting convergence.

Furthermore, when both concentrations are changed in an injection, the derivatives $(\partial n/\partial w_i)_{w_j}$, $(i \neq j)$ change values as the quantity in the subscript w_j is not constant anymore. We have found out that by varying Δw_i it is possible to find combinations of Taylor peaks with slightly better optical sensitivity such that the fitting procedure converges better.

Fitting procedure

An unconstrained Nelder-Mead (simplex) method available in Matlab, similar to that employed by Mialdun *et al.*[35], was used for the fitting of experimental refractive index detector voltage data with working equations. Instead of direct fitting of the coefficients D_{11}^V, D_{12}^V, D_{21}^V and D_{22}^V, the procedure suggested by Ray and Leaist[45] was used. A peak signal was normalized such that Eq. (32) takes the form

$$V(t) = \sum_{i=0}^{m} \zeta_i t^i + \Delta V_{max} \sqrt{\frac{t_R}{t}} \left[W_1 \exp(-\hat{D}_1 \eta) + (1 - W_1) \exp(-\hat{D}_2 \eta) \right] , \tag{35}$$

where W_1 is the normalized weight

$$W_1 = \frac{(a + b\alpha)\sqrt{\hat{D}_1}}{(a + b\alpha)\sqrt{\hat{D}_1} + (1 - a - b\alpha)\sqrt{\hat{D}_2}} , \tag{36}$$

and the parameters are

$$a = \frac{D_{11}^V - \hat{D}_1 - S_R D_{12}^V}{(\hat{D}_2 - \hat{D}_1)} , \tag{37}$$

$$b = \frac{D_{22}^V - D_{11}^V - D_{21}^V / S_R + S_R D_{12}^V}{(\hat{D}_2 - \hat{D}_1)} , \tag{38}$$

$$\alpha = \frac{\Delta w_1}{\Delta w_1 + \Delta w_2 (M_1/M_2)/S_R} . \tag{39}$$

The Fick diffusion coefficients were calculated from the fit parameters $\hat{D}_1$, $\hat{D}_2$, a and b as follows[45]

$$D_{11}^V = \hat{D}_1 + \frac{a(1-a-b)}{b}(\hat{D}_1 - \hat{D}_2) \,, \tag{40}$$

$$D_{12}^V = \frac{1}{S_R}\frac{a(1-a)}{b}(\hat{D}_1 - \hat{D}_2) \,, \tag{41}$$

$$D_{21}^V = S_R\frac{(a+b)(1-a-b)}{b}(\hat{D}_2 - \hat{D}_1) \,, \tag{42}$$

$$D_{22}^V = \hat{D}_2 + \frac{a(1-a-b)}{b}(\hat{D}_2 - \hat{D}_1) \,. \tag{43}$$

Note that there is a misprint of signs in Eq. (38) in the original paper[45].

Molecular Simulation

The Fick diffusion coefficient matrix was determined consistently by means of molecular simulation. *I.e.*, both the MS diffusion coefficient and the thermodynamic factor matrices were computed exclusively on the basis of simulation data. For this purpose, rigid, united-atom type models were used to describe the intermolecular interactions. The molecular models employed in this work[46–48] account for these interactions, including hydrogen-bonding, by a set of Lennard-Jones (LJ) sites and point charges which may or may not coincide with the LJ site positions. The molecular models for methanol and ethanol were taken from prior work[46,47]. For water, the TIP4P/2005 model by Abascal and Vega[48] was used. These models were satisfactorily assessed in previous works with respect to the binary subsystems of the ternary mixture under consideration[6,14]. The interested reader is referred to the original publications[46–48] for detailed information about the three molecular pure substance models and their parameters.

To define a molecular model for a ternary mixture on the basis of pairwise additive pure substance models, only the unlike interactions have to be specified. In case of polar interaction sites, *i.e.*, point charges here, this can straightforwardly be done using the laws of electrostatics. However, for the unlike LJ parameters, there is no physically sound approach so that combining rules have to be employed for predictions. Therefore, the simple Lorentz-Berthelot combining rule was

chosen. Because not a single experimental data point on mixture properties or on transport properties was considered in the model parameterization, the mixture data from molecular simulation presented below are strictly predictive.

Methodology

The Green-Kubo formalism based on the net velocity auto-correlation function[26]

$$L_{ij} = \frac{1}{3N_p} \int_0^\infty \mathrm{d}t \left\langle \sum_{k=1}^{N_{p,i}} \mathbf{v}_{i,k}(0) \cdot \sum_{l=1}^{N_{p,j}} \mathbf{v}_{j,l}(t) \right\rangle , \tag{44}$$

was used here to calculate the MS diffusion coefficients. N_p is the total number of molecules, $N_{p,i}$ is the number of molecules of component i and $\mathbf{v}_{i,k}(t)$ denotes the center of mass velocity vector of the k-th molecule of component i at time t. Note that Eq. (44) corresponds to a reference frame in which the mass-averaged mixture velocity is zero[26].

For a ternary mixture, the elements of the inverse matrix $\mathbf{B}^{-1}$ in the molar-averaged frame of reference, cf. Eqs. (10) and (11), are given by[26]

$$\begin{aligned}
B_{11}^{-1} &= (1-x_1)\left(\frac{L_{11}}{x_1} - \frac{L_{13}}{x_3}\right) - x_1\left(\frac{L_{21}}{x_1} - \frac{L_{23}}{x_3} + \frac{L_{31}}{x_1} - \frac{L_{33}}{x_3}\right), \\
B_{12}^{-1} &= (1-x_1)\left(\frac{L_{12}}{x_2} - \frac{L_{13}}{x_3}\right) - x_1\left(\frac{L_{22}}{x_2} - \frac{L_{23}}{x_3} + \frac{L_{32}}{x_2} - \frac{L_{33}}{x_3}\right), \\
B_{21}^{-1} &= (1-x_2)\left(\frac{L_{21}}{x_1} - \frac{L_{23}}{x_3}\right) - x_2\left(\frac{L_{11}}{x_1} - \frac{L_{13}}{x_3} + \frac{L_{31}}{x_1} - \frac{L_{33}}{x_3}\right), \\
B_{22}^{-1} &= (1-x_2)\left(\frac{L_{22}}{x_2} - \frac{L_{23}}{x_3}\right) - x_2\left(\frac{L_{12}}{x_2} - \frac{L_{13}}{x_3} + \frac{L_{32}}{x_2} - \frac{L_{33}}{x_3}\right).
\end{aligned} \tag{45}$$

The three MS diffusion coefficients can be calculated with

$$
\begin{aligned}
Đ_{13} &= \frac{1}{B_{11} + B_{12} \cdot (x_2/x_1)}\,, \\
Đ_{12} &= \frac{1}{B_{11} - B_{12} \cdot (x_1 + x_3)/x_1}\,, \\
Đ_{23} &= \frac{1}{B_{22} + B_{21} \cdot (x_1/x_2)}\,.
\end{aligned} \tag{46}
$$

During EMD simulation runs, the intra-diffusion coefficients were sampled simultaneously. The corresponding Green-Kubo equation can be found, *e.g.*, in Ref.[6].

In the present work, the thermodynamic factor was calculated following its definition (12). The chemical potentials, and thus the activity coefficients, were sampled by MC simulation on the basis of the same molecular force field models. The derivatives of the activity coefficients at constant temperature and pressure were subsequently obtained from a fit of the simulation results using a thermodynamic model. Having the thermodynamic factor, the MS diffusion coefficients, as determined by EMD, were transformed to the Fick diffusion coefficients according to Eq. (10).

Sampling the chemical potential by simulation is often a difficult task for dense liquids, requiring advanced techniques. However, in previous work[6] it was shown that with an appropriate method and suitably chosen parameters, the composition profile of the chemical potential can be obtained by relatively inexpensive MC simulations with at least the same precision as with the method based on experimental VLE data.

The chemical potential μ_i of component i can be separated into the solely temperature dependent ideal contribution $\mu_i^{\mathrm{id}}(T)$ and the remaining contribution $\tilde{\mu}_i(T,p,\boldsymbol{x}) \equiv \mu_i(T,p,\boldsymbol{x}) - \mu_i^{\mathrm{id}}(T)$. This contribution contains the desired $\ln\gamma_i$ term that appears in Eq. (12). In this way, the mole fraction derivative of the activity coefficient can be written as

$$
\left.\frac{\partial \ln\gamma_i}{\partial x_j}\right|_{T,p,x_{k,k\neq j=1\ldots N-1}} = \left.\frac{\partial(\beta\tilde{\mu}_i - \ln x_i)}{\partial x_j}\right|_{T,p,x_{k,k\neq j=1\ldots N-1}}\,. \tag{47}
$$

This derivative was calculated analytically from the Wilson model that was fitted to simulation

data. The thermodynamic factor is then given by[28]

$$\Gamma_{ij} = \delta_{ij} + x_i(Q_{ij} - Q_{iN}), \tag{48}$$

and

$$Q_{ij} = -\Lambda_{ij}/S_i - \Lambda_{ji}/S_j + \sum_{k=1}^{N} x_k \Lambda_{ki}\Lambda_{kj}/S_k^2, \tag{49}$$

where S_i is a function of Λ_{ij} and composition. Λ_{ij} are adjustable Wilson parameters and their numerical values are given in Ref.[6]. Note that this multicomponent thermodynamic model defines also the properties of its binary subsystems.

Results and discussion

Experiment

The main elements of the Fick diffusion coefficient matrix monotonically grow with increasing methanol content along path A, while $D_{11}^V < D_{22}^V$, as seen in Fig. 4a. The cross elements of the diffusion matrix shown in Fig. 4b are negative and essentially smaller than the main terms; over that path $|D_{12}^V|$ is slightly larger than $|D_{21}^V|$. A negative cross element of the diffusion matrix D_{ij}^V implies that species i diffuses towards larger concentrations of species j.

The experiment was originated on path B (state point #1) and the fitting procedure for path A began at the intersection of two paths, then it moved up and down. Unlike other mixtures[34,37], the convergence of the fitting routine deteriorates approaching the binary limits along path A. In the limit $w_2 \to 0$ the cross diffusion coefficient D_{21}^V should tend towards zero, whereas D_{11}^V should reach the limit of the binary Fick diffusion coefficient of the water-ethanol subsystem $D_{bin}^{w_1-w_3}$. Numerous repetitions of the experiment at state point #11 provided two stable solutions: one of them is indicated in Table 3 and the another one corresponds to similar eigenvalues (D_{11}^V=1.11; D_{12}^V=-0.017, D_{21}^V=-0.007; D_{22}^V =1.14 in units of 10^{-9}m^2/s). This ambiguity is in line with observations

for the binary mixture water-ethanol. The majority of experiments on binary diffusion in water-ethanol with a mass relation 0.1/0.9 reported a diffusion coefficient of $D_{bin}^{w_1-w_3} = 0.88 \cdot 10^{-9}$ m^2/s[34] which is shown as a blue diamond in Fig. 4a. However, there is another result $D_{bin}^{w_1-w_3} = 0.65 \cdot 10^{-9}$ m^2/s in the literature[49] which is depicted in Fig. 4a as a blue open circle. Asymptotically, the former binary diffusion coefficient corresponds to the ternary system with similar eigenvalues and the latter one to the ternary coefficients presented above. This indeterminacy can be attributed to recent experimental studies on binary mixtures of concentrated low molar weight alcohols and water, which have demonstrated incomplete mixing at the molecular level in alcohol-water systems[1].

At the other end of the concentration path, *i.e.*, $w_3 \to 0$, the observations are even more intriguing. The measured binary diffusion coefficient at state point #19 scattered in the range of $(1.75 - 2.8) \cdot 10^{-9}$ m^2/s. The solution of that enigma becomes evident when one of the experiments revealed a peak with dips, similar to that in Fig. 3b. Such a peak identifies two different kinetics in the liquid system which are possible only in ternary or higher mixtures. Thus, our experiment for the first time presented an evidence on the macroscopic scale that a binary system may behave as a ternary system due to clustering.

The results of the Taylor dispersion measurements for the main diffusion coefficients D_{11}^V and D_{22}^V along path B are shown in Fig. 5a. The open symbols indicate the asymptotic values of the coefficient near the binary limits. The first observation at both ends of path B is that our measurements perfectly meet the expectations at the binary limits. Indeed, the asymptotic quantity derived in Eq. (23) is equal to $[D_{22}^V - D_{21}^V(M_2/M_1)] = 0.9 \cdot 10^{-9}$m^2/s, while the measured binary diffusion coefficient on the right hand side (state point #9, w_1=0.56 kg kg^{-1}) is $D_{bin}^{w_1-w_2} = 0.94 \cdot 10^{-9}$m^2/s. The second asymptotic quantity, expressed by Eq. (24), tends to zero and the coefficient D_{11}^V obtained from this expression is in excellent agreement with the measured value.

Near the binary limits, the reproducibility of the results was excellent in terms of the pseudo-binary diffusion coefficients and convergence to the same solution regardless of the initial guess. The calculated relative uncertainty, *i.e.*, the standard deviation divided by the average value, yields coherent results of about 2% which can be applied to mass fractions $w_1 < 0.1$ kg kg^{-1} and $w_1 > 0.3$

kg kg^{-1}. However, along path B the uncertainty of the measured diffusion coefficients increases due to the poor optical properties of the mixture discussed above. This region of poor contrast is indicated by a shadow in Fig. 5.

The cross diffusion coefficients presented in Fig. 5b show a very different behavior along path B: relatively large negative D_{12}^V values and small D_{21}^V values that change sign in the middle of the path. It is worth noting that in line with the asymptotic predictions, $D_{12}^V \to 0$ was found on the left hand side of the triangle. Again, the coefficients are strongly dispersed around the trend curve in the region with poor optical properties.

The numerical results for the diffusion coefficients measured by Taylor dispersion in the ternary mixture are listed in Table 3.

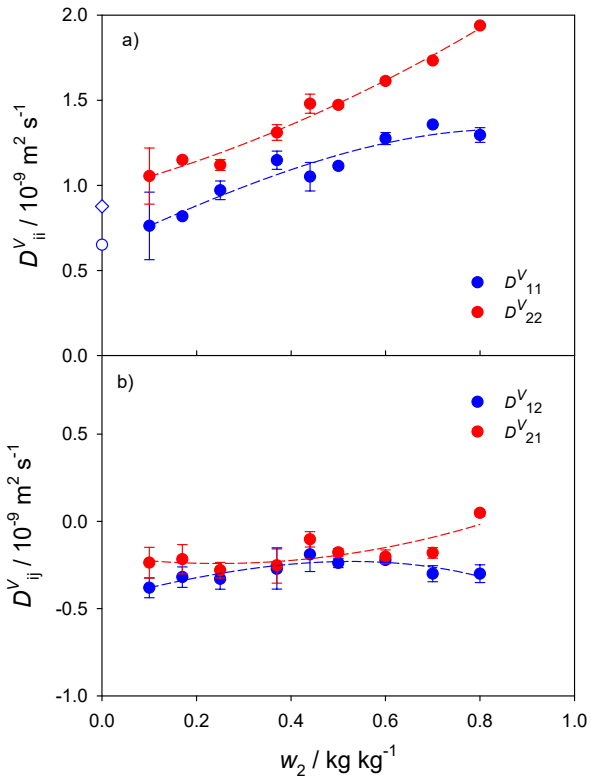

Figure 4: (a) Measured main elements D_{11}^V, D_{22}^V and (b) cross elements D_{12}^V, D_{21}^V of the Fick diffusion coefficient matrix along path A in the mixture water (1) + methanol (2) + ethanol (3). The open symbols indicate asymptotic values approaching the binary subsystem from Ref.[34] (circle) and Ref.[49] (diamond). The dotted lines are given as a guide for the eyes.

Table 3: Measured Fick diffusion coefficients $D_{ij}^V/10^{-9}\mathrm{m}^2\mathrm{s}^{-1}$ and their uncertainties $\sigma/10^{-9}\mathrm{m}^2\mathrm{s}^{-1}$ for the mixture water (1) + methanol (2) + ethanol (3) at 298.15 K and 0.1 MPa along path A ($w_1 = 0.1$ kg kg^{-1}) and path B ($w_2 = 0.44$ kg kg^{-1}). The degree of asymmetry δ_{Ons} (%) according to Eq. (17) is also given.

Point #	w_1	w_2	w_3	D_{11}^V	σ	D_{12}^V	σ	D_{21}^V	σ	D_{22}^V	σ	δ_{Ons}
						Path A						
10	0.10	0.00	0.90	0.877	0.018							
11	0.10	0.10	0.80	0.762	0.199	-0.381	0.057	-0.237	0.088	1.055	0.165	-38.9
12	0.10	0.17	0.73	0.818	0.008	-0.320	0.058	-0.217	0.083	1.150	0.008	-5.2
13	0.10	0.25	0.65	0.971	0.047	-0.330	0.055	-0.280	0.045	1.120	0.032	-2.3
14	0.10	0.37	0.53	1.178	0.063	-0.273	0.115	-0.253	0.102	1.311	0.046	5.4
15	0.10	0.50	0.40	1.114	0.014	-0.238	0.027	-0.178	0.022	1.473	0.014	12.2
16	0.10	0.60	0.30	1.275	0.035	-0.222	0.014	-0.203	0.039	1.613	0.008	2.9
17	0.10	0.70	0.20	1.357	0.002	-0.300	0.046	-0.181	0.030	1.733	0.002	4.1
18	0.10	0.80	0.10	1.296	0.043	-0.300	0.051	0.048	0.018	1.939	0.007	5.3
19	0.10	0.90	0.00							2.250	0.430	
						Path B						
1	0.00	0.44	0.56							1.684		
2	0.03	0.44	0.53	1.625	0.005	-0.040	0.052	-0.132	0.013	1.562	0.009	5.8
3	0.10	0.44	0.46	1.051	0.084	-0.189	0.098	-0.103	0.044	1.480	0.056	19.3
4	0.20	0.44	0.36	1.069	0.151	-0.594	0.156	-0.065	0.061	1.067	0.150	27.2
5	0.25	0.44	0.31	0.695	0.168	-0.630	0.134	0.083	0.030	1.351	0.133	45.6
6	0.30	0.44	0.26	0.745	0.019	-0.422	0.122	0.019	0.007	1.194	0.007	13.3
7	0.40	0.44	0.16	0.737	0.013	-0.359	0.078	0.038	0.011	1.116	0.010	4.1
8	0.50	0.44	0.06	0.639	0.016	-0.336	0.148	0.157	0.057	1.165	0.016	6.4

Table 4: Eigenvalues $\hat{D}_1$ and $\hat{D}_2$ in units of $10^{-9}\mathrm{m}^2\mathrm{s}^{-1}$ along path A ($w_1 = 0.1$ kg kg^{-1}) and path B ($w_2 = 0.44$ kg kg^{-1}) at 298.15 K and 0.1 MPa from experiments and predicted by molecular simulation.

Point #	w_1	w_2	w_3	$\hat{D}_1^{\mathrm{exp}}$	$\hat{D}_2^{\mathrm{exp}}$	$\hat{D}_1^{\mathrm{sim}}$	$\hat{D}_2^{\mathrm{sim}}$
Path A							
11	0.10	0.10	0.80	1.243	0.574	1.103	0.751
12	0.10	0.17	0.73	1.295	0.673	1.175	0.853
13	0.10	0.25	0.65	1.358	0.733	1.198	0.854
14	0.10	0.37	0.53	1.515	0.973	1.341	1.024
3	0.10	0.44	0.46	1.522	1.010	1.393	1.018
15	0.10	0.50	0.40	1.567	1.021	1.434	1.123
16	0.10	0.60	0.30	1.716	1.173	1.559	1.189
17	0.10	0.70	0.20	1.845	1.246	1.592	1.250
18	0.10	0.80	0.10	1.915	1.320	1.689	1.476
Path B							
2	0.03	0.44	0.53	1.672	1.514	1.750	1.326
3	0.10	0.44	0.46	1.522	1.010	1.393	1.018
4	0.20	0.44	0.36	1.264	0.871	1.267	0.870
5	0.25	0.44	0.31	1.260	0.787	1.237	0.800
6	0.30	0.44	0.26	1.175	0.764	1.154	0.782
7	0.40	0.44	0.16	1.076	0.777	1.089	0.705
8	0.50	0.44	0.06	1.031	0.774	1.037	0.730

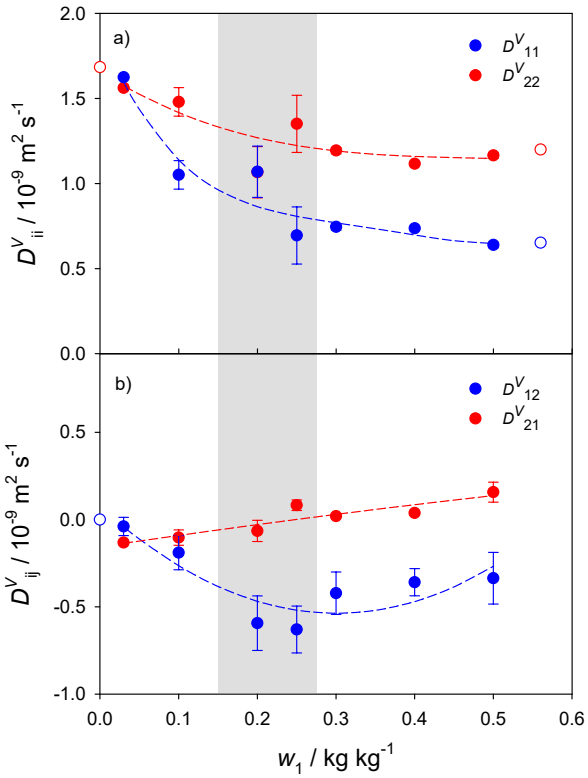

Figure 5: (a) Measured main elements D^V_{11}, D^V_{22} and (b) cross elements D^V_{12}, D^V_{21} of the Fick diffusion coefficient matrix along path B in the mixture water (1) + methanol (2) + ethanol (3). The open symbols indicate asymptotic values approaching the binary subsystem from present experiments. Poor optical properties were encountered in the shaded composition range. The dotted lines are given as a guide for the eyes.

Verification of the Onsager reciprocal relations

The experimental verification of the Onsager reciprocal relations (ORR) for ternary diffusion are dated back to 1960[50]. That examination was carried out on the basis of diffusion coefficient data for ten different aqueous salt solutions (KCl, NaCl, LiCl) or raffinose. Since then, published data on the experimental verification of ORR are rare. We have checked the validity of ORR at all measured state points, although the procedure is not straightforward. The diffusion coefficients were measured in the volume-averaged frame of reference and then converted to the molar-averaged frame of reference by Eq. (5). The required partial molar volumes and the thermodynamic matrix **G** are known with some uncertainty which could influence the degree of asymmetry defined by Eq. (17). The numerical values for these quantities are given in the Appendix B. Furthermore, it was noted above that the measurement of diffusion coefficients at some state points of this mixture was particularly difficult. Still, the correct qualitative behavior is expected to be captured.

The degree of asymmetry of the ORR is given in the last column of Table 3 and it follows that the ORR are fulfilled within acceptable error limits. The value of the misfit is in accordance with the quality of the results for the diffusion coefficients discussed above. Along path A the ORR are satisfied within error limits smaller than 5.3% with the exception of state points #11 and #15. It should be recalled that at the problematic state point #11 there is a second solution for which the ORR are satisfied with $\delta_{\mathrm{Ons}}(\%) = 0.25\%$ and that state point #15 falls into the region where the optical properties start to decline.

Along path B the ORR are satisfied within an error depending on the quality of the optical properties of the mixture. The largest uncertainty was observed in the region with the poorest optical contrast (state point #5) and then decreases down to 4%.

Simulation

Predictive molecular simulations were carried out at 298.15 K and 0.1 MPa along paths A and B as depicted in Fig. 1. Moreover, 12 additional state points were sampled to cover the remaining ternary composition range of the ternary liquid mixture.

The thermodynamic factor matrix was obtained from the Wilson G^{E} model fitted to the chemical potential data from molecular simulation using Eqs. (48) and (49). The systematic error introduced by that fit was estimated to be less than 5% in magnitude. The MS diffusion coefficients were obtained with EMD and the Green-Kubo formalism and the Fick diffusion coefficient matrix based on the molar-averaged frame of reference was calculated using Eq. (10). The numerical simulation results for the predicted molar density, MS diffusion coefficients and the thermodynamic factor matrices are listed in table 5 for all regarded state points. The Fick diffusion coefficient matrix is given for paths A and B in table 6. All simulation results are consistent and their numerical values for $\mathbf{D}^M$ fulfill the theoretical restrictions for thermodynamic stability given by Taylor and Krishna[21], *i.e.*, $\mathbf{D}^M$ has positive and real eigenvalues, positive diagonal elements and a positive determinant.

Usually, the main Fick diffusion coefficients D_{ii}^M are larger than the cross elements D_{ij}^M ($i \neq j$), which is expected as the diffusive flow of component i is mainly driven by its own concentration gradient[51]. Coupling effects described by the relation between the diffusion coefficients D_{21}^M and D_{22}^M are not important. On the other hand, the absolute numerical values of the cross diffusion coefficient D_{12}^M can be more important than the main term D_{11}^M, especially for state points #7 and #8, suggesting larger coupling effects, which may be caused by the presence of strong non-idealities. Further, D_{22}^M is always larger than D_{11}^M, D_{12}^M is negative throughout and D_{21}^M can be positive or reach small negative values depending on mixture composition.

Fig. 6 shows a fit of the simulation results for the four Fick diffusion coefficients in the molar-averaged frame of reference for the studied mixture over the whole composition range. As can be seen, the surfaces for the four different coefficients behave differently. D_{11}^M is always positive but can achieve values up to six times lower than its maximum value. The values of D_{22}^M exhibit a smaller variation than that of D_{11}^M, reaching values only twice as low as their maximum. D_{21}^M varies from positive to negative and D_{21}^M is always negative.

Table 7 shows the comparison of the predictions made by molecular simulation here and in previous work[6]. Although the same force field models were used, the values are not expected to be

Table 5: Molar density ρ^M / mol l^{-1}, Maxwell-Stefan diffusion coefficients $Đ_{ij}/10^{-9}$m^{2}s^{-1} together with their statistical uncertainties $\sigma/10^{-9}$m^{2}s^{-1} and the thermodynamic factor matrix of the ternary system water (1) + methanol (2) + ethanol (3) at 298.15 K and 0.1 MPa predicted by molecular simulation.

x_1	x_2	x_3	ρ^M	$Đ_{13}$	σ	$Đ_{12}$	σ	$Đ_{23}$	σ	Γ_{11}	Γ_{12}	Γ_{21}	Γ_{22}
0.062	0.510	0.428	21.40	1.422	0.39	1.453	0.40	1.724	0.10	0.919	-0.021	-0.031	1.032
0.190	0.469	0.341	23.84	1.223	0.29	1.457	0.44	1.298	0.14	0.760	-0.062	0.072	1.057
0.340	0.421	0.239	27.40	1.271	0.27	1.634	0.54	1.025	0.17	0.588	-0.104	0.205	1.086
0.404	0.400	0.196	29.20	1.282	0.27	1.530	0.47	1.023	0.19	0.520	-0.121	0.269	1.100
0.462	0.381	0.157	31.04	1.371	0.30	1.661	0.55	0.827	0.18	0.461	-0.136	0.333	1.114
0.563	0.349	0.088	34.82	1.292	0.32	1.708	0.75	0.695	0.20	0.368	-0.164	0.468	1.143
0.649	0.321	0.030	38.72	1.435	0.44	1.653	0.80	0.619	0.26	0.300	-0.188	0.621	1.178
0.213	0.120	0.667	21.22	1.044	0.13	1.040	0.44	1.092	0.17	0.718	-0.070	0.002	1.022
0.208	0.199	0.593	21.76	1.154	0.18	1.282	0.52	1.096	0.15	0.728	-0.068	0.011	1.034
0.202	0.284	0.514	22.37	1.135	0.20	1.192	0.40	1.142	0.14	0.738	-0.066	0.026	1.043
0.194	0.404	0.402	23.29	1.326	0.27	1.389	0.38	1.254	0.14	0.752	-0.063	0.053	1.053
0.186	0.523	0.291	24.29	1.405	0.35	1.475	0.36	1.351	0.15	0.765	-0.060	0.089	1.059
0.180	0.608	0.212	25.05	1.313	0.37	1.631	0.43	1.474	0.15	0.775	-0.058	0.117	1.059
0.175	0.688	0.137	25.83	1.484	0.50	1.544	0.34	1.562	0.17	0.783	-0.057	0.146	1.059
0.170	0.764	0.066	26.59	1.671	0.74	1.803	0.42	1.641	0.20	0.791	-0.055	0.174	1.057
0.40	0.10	0.50	25.18	1.047	0.12	1.481	0.78	0.828	0.17	0.511	-0.118	0.043	1.032
0.40	0.25	0.35	27.01	1.326	0.21	1.351	0.39	0.796	0.15	0.519	-0.119	0.137	1.071
0.40	0.50	0.10	30.63	1.370	0.37	1.705	0.58	1.045	0.22	0.527	-0.120	0.362	1.112
0.60	0.10	0.30	31.71	1.173	0.12	1.234	0.39	0.615	0.16	0.334	-0.166	0.118	1.057
0.60	0.25	0.15	34.54	1.316	0.22	1.514	0.49	0.650	0.16	0.337	-0.171	0.359	1.125
0.80	0.10	0.10	42.13	1.067	0.14	1.554	0.66	0.504	0.16	0.250	-0.216	0.315	1.123
0.10	0.20	0.70	19.79	1.204	0.22	0.927	0.36	1.303	0.12	0.863	-0.035	-0.027	1.022
0.10	0.40	0.50	21.27	1.297	0.31	1.427	0.50	1.297	0.11	0.868	-0.034	-0.017	1.036
0.10	0.60	0.30	22.99	1.256	0.36	1.718	0.51	1.594	0.12	0.872	-0.034	0.023	1.041
0.30	0.20	0.50	23.76	1.228	0.18	1.301	0.44	0.969	0.16	0.622	-0.093	0.050	1.046
0.30	0.30	0.40	24.82	1.013	0.19	1.289	0.50	1.058	0.17	0.627	-0.093	0.093	1.061
0.30	0.50	0.20	27.19	1.373	0.33	1.616	0.46	1.131	0.17	0.634	-0.093	0.210	1.084

Table 6: Predicted Fick diffusion coefficients $D_{ij}^{M}/10^{-9}\mathrm{m}^2\mathrm{s}^{-1}$ and their statistical uncertainties $\sigma/10^{-9}\mathrm{m}^2\mathrm{s}^{-1}$ for the mixture water (1) + methanol (2) + ethanol (3) at 298.15 K and 0.1 MPa along path A ($w_1 = 0.1$ kg kg^{-1}) and path B ($w_2 = 0.44$ kg kg^{-1}) from molecular simulation.

Point #	x_1	x_2	x_3	D_{11}^{M}	σ	D_{12}^{M}	σ	D_{21}^{M}	σ	D_{22}^{M}	σ
						Path A					
11	0.213	0.120	0.667	0.749	0.060	-0.072	0.086	0.007	0.042	1.104	0.058
12	0.208	0.199	0.593	0.858	0.072	-0.105	0.076	-0.013	0.061	1.171	0.063
13	0.202	0.284	0.514	0.849	0.078	-0.088	0.070	0.019	0.078	1.203	0.068
14	0.194	0.404	0.402	1.016	0.092	-0.097	0.068	0.027	0.097	1.350	0.074
15	0.186	0.523	0.291	1.102	0.098	-0.100	0.072	0.072	0.125	1.457	0.087
16	0.180	0.608	0.212	1.150	0.117	-0.151	0.078	0.107	0.148	1.598	0.097
17	0.175	0.688	0.137	1.192	0.135	-0.098	0.090	0.237	0.177	1.650	0.113
18	0.170	0.764	0.066	1.397	0.178	-0.120	0.116	0.193	0.219	1.769	0.142
						Path B					
2	0.062	0.510	0.428	1.321	0.102	-0.033	0.041	0.071	0.189	1.756	0.073
3	0.190	0.469	0.341	1.003	0.101	-0.128	0.071	0.043	0.123	1.407	0.082
4	0.340	0.421	0.239	0.817	0.096	-0.256	0.093	0.094	0.093	1.321	0.090
5	0.404	0.400	0.196	0.698	0.099	-0.260	0.099	0.211	0.092	1.339	0.098
6	0.462	0.381	0.157	0.661	0.102	-0.310	0.104	0.194	0.091	1.276	0.102
7	0.563	0.349	0.088	0.467	0.115	-0.430	0.135	0.344	0.109	1.327	0.116
8	0.649	0.321	0.030	0.405	0.178	-0.403	0.188	0.510	0.170	1.362	0.184

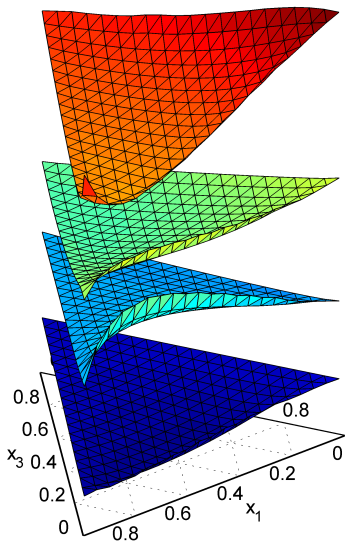

Figure 6: Qualitative behavior of the Fick diffusion coefficients D_{11}^M (red), D_{22}^M (green), D_{21}^M (light blue) and D_{12}^M (dark blue) predicted by molecular simulation over the whole composition range for the mixture water (1) + methanol (2) + ethanol (3). The surfaces were shifted vertically to avoid intersections and maintain visibility.

identical, because the simulation conditions with respect to system size and sampled time differed. Nevertheless, the values agree within the combined statistical uncertainties of both simulation efforts.

Intra-diffusion coefficients

The analysis of the intra-diffusion coefficients of the components in a mixture may lead to a better understanding of the collective diffusive behavior. Further, these coefficients can be obtained basically without additional computational effort from EMD. Fig. 7 shows the composition dependence of the intra-diffusion coefficients along paths A and B. In an ideal mixture, the component with the lowest molecular weight is expected to have the highest intra-diffusion coefficient, *i.e.*, to propagate faster than the other components. However, water, which is by far the lightest and smallest molecule, has a intra-diffusion coefficient that is almost identical with that of ethanol, a molecule with 2.5 times its molecular weight. Thus, the effective diffusion diameter[52] of water molecules has to be higher than that of the single molecule, indicating the presence of water inside

Table 7: Present simulation results for the Fick diffusion coefficients $D_{ij}^{M}/10^{-9}\mathrm{m}^2\mathrm{s}^{-1}$ compared with predictions from preceding work[6] for the mixture water (1) + methanol (2) + ethanol (3) at 298.15 K and 0.1 MPa.

x_1	x_2	x_3	D_{11}^{M}	D_{12}^{M}	D_{21}^{M}	D_{22}^{M}	Source
0.33	0.33	0.34	0.725	-0.258	0.060	1.167	This work
			0.80	-0.12	0.03	1.05	Ref.[6]
0.20	0.40	0.40	0.993	-0.106	0.028	1.331	This work
			0.90	-0.09	0.04	1.24	Ref.[6]
0.40	0.20	0.40	0.594	-0.239	0.059	1.172	This work
			0.51	-0.25	0.10	1.21	Ref.[6]
0.40	0.40	0.20	0.698	-0.260	0.211	1.339	This work
			0.63	-0.26	0.22	1.29	Ref.[6]
0.20	0.20	0.60	0.854	-0.113	-0.017	1.176	This work
			0.89	0.02	0.03	0.99	Ref.[6]
0.20	0.60	0.20	1.206	-0.216	0.001	1.529	This work
			0.95	-0.21	0.28	1.72	Ref.[6]
0.60	0.20	0.20	0.363	-0.371	0.279	1.237	This work
			0.44	-0.43	0.16	1.17	Ref.[6]

clusters. This phenomenon was observed at low water concentrations, *i.e.*, along the entire path A and for path B at $w_1 < 0.1$ kg kg^{-1}. At higher water concentrations, the intra-diffusion coefficient of water increases with respect to that of ethanol, *i.e.*, the effective diffusion diameter and the size of the water clusters decreases. Clustering of water molecules can clearly be seen in the molecular simulation snapshots for state point #18 shown in Fig. 8. Note that present experiments have shown evidence of the presence of clustering in the neighboring binary state point #19.

Comparison of experiment and simulation

Fig. 9 shows present predictions of the Fick diffusion coefficient matrix by molecular simulation compared with present experimental values along path A. The Fick diffusion coefficient data in the volume-averaged frame of reference obtained with the Taylor dispersion technique were converted to the molar-averaged frame of reference using Eqs. (5), (6) and (8). For this purpose, the experimental excess volume data by Zarei et al.[25] and their fitting parameters[25] were employed,

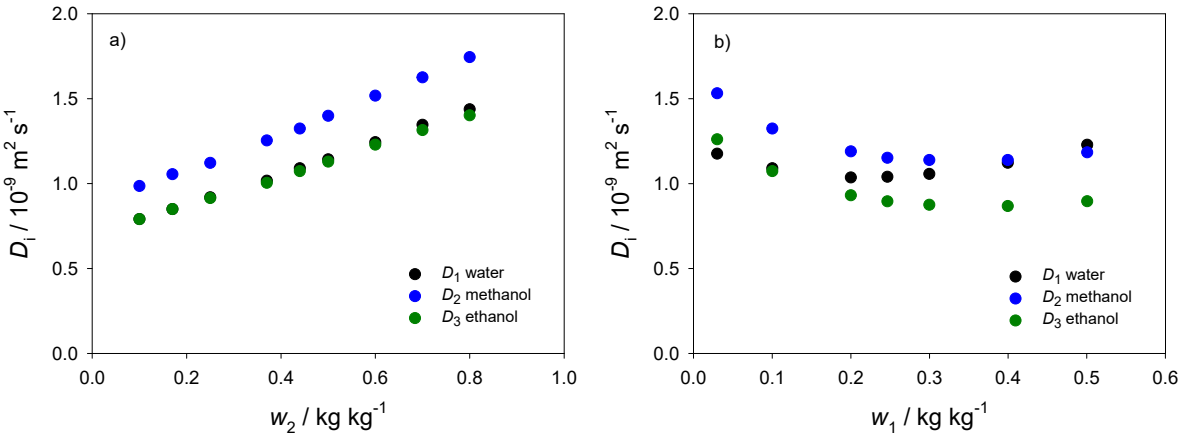

Figure 7: Simulation results of the intra-diffusion coefficients of water, methanol and ethanol in their ternary mixture along (a) path A and (b) path B. The statistical uncertainties are within symbol size.

who modeled the excess volume of the ternary mixture with a Cibulka equation[53] and the required binaries with a Redlich-Kister type equation[25]. (Note that there is a typo with respect with the sign of two of the given equation constants in the work of Zarei et al.[25]).

As can be seen in Figs. 9 and 10 there is a very good agreement between the simulation results and the experimental data for the main elements of the Fick diffusion matrix along both paths. Typically, simulation and experiment agree within their uncertainties, with average absolute deviations of 15% and 8% for D_{11}^M and D_{22}^M, respectively. Looking at the main Fick diffusion coefficients along path A, it can be concluded that, in general, they have the same tendency to increase with methanol content. The coefficient D_{11}^M does not correspond to the trend of the remaining experimental data only for a single state point, *i.e.*, #18. It can also be seen that the composition dependence of the main coefficient D_{22}^M predicted by molecular simulation starts to diverge from the measured one for concentrations $w_2 > 0.5$ kg kg^{-1}. This difference slowly grows with increasing methanol content to reach an overestimation of around 10% at the end of path A, cf. Fig. 9d. As previously discussed in the experimental section, in the methanol-rich region, the diffusion coefficients even for binary mixtures (*e.g.*, at state point #19) show ambiguous behavior which can be attributed to clustering. On the side, at low methanol content, the experimental and calculated values of D_{11}^M are consistent with the expected asymptotic behavior in the limit $w_2 \to 0$ while approaching the binary diffusion

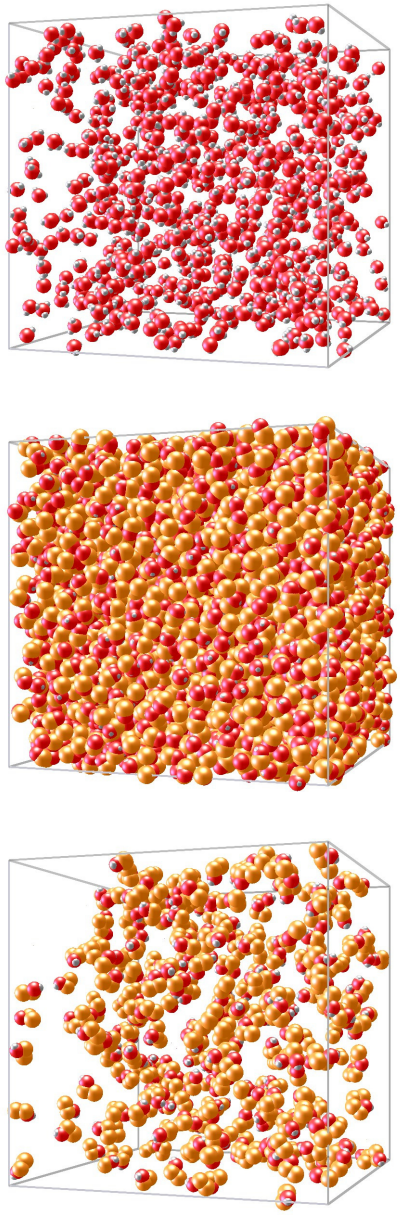

Figure 8: Snapshot of water + methanol + ethanol at state point #18. To improve visibility, only one type of molecule is shown at a time, *i.e.*, water (top), methanol (center) or ethanol (bottom). The methyl and methylene groups are shown in orange, the oxygen atoms in red and the hydroxyl hydrogen atoms in white.

coefficient of the water-ethanol subsystem reported in Ref.[49].

Along path B, cf. Fig. 10, for the main diffusion coefficients there are no significant differences between experimental and simulation results. Both coefficients, D_{11}^M and D_{22}^M, decrease with the increase of water content and the decreasing rate is stronger for D_{11}^M. It can be noticed that the experimental value at state point #5 is inconsistent with the remaining experimental data for all coefficients. The explanation can be found in Fig. 2b, indicating that this state point is near the maximum of the parabolic-type curve $n(w_1)$. The poor optical properties in this region give priority to the simulation data in terms of reliability of the numerical values of the coefficients. This situation demonstrates that molecular simulation is not just a simple companion to experiment, but being validated, it supports the efficiency of experiments in hard to reach areas. However, at the beginning of path B the predicted value for state point #2 seems to be too large, since it does not follow the expected asymptotic behavior towards the binary subsystem, *i.e.*, in the limit $w_1 \to 0$, where D_{22}^M should approach the binary diffusion coefficient of the subsystem methanol-ethanol.

The qualitative agreement of the cross elements of the diffusion matrix is very good, however, because of their rather small values, the scatter of the experimental results and the large statistical uncertainties of the simulations, the quantitative agreement is not as good as for the main coefficients, leading to absolute average deviations above 50%, cf. Figs. 9 and 10. Along path A, simulation and experiment yield negative values for D_{12}^M, however, the predictions by molecular simulation are systematically higher than the experimental results. In case of D_{21}^M, again, the predictions by molecular simulation are generally higher than the experimental results, but the simulation results are more consistent with the expected asymptotic behavior than the experimental values, *i.e.*, $D_{21} \to 0$ in the limit $w_2 \to 0$, cf. Fig. 9c. The agreement of experiment and simulation for both cross elements of the diffusion matrix along path B is better than along path A. Further, the asymptotic behavior towards the binary subsystem, *i.e.*, $D_{12} \to 0$, is predicted well. Again, there is a problem with the agreement at state point #5 for D_{12}^M and D_{21}^M between experiment and simulation. However, as can be seen in Fig. 10, the experimental values for this state point do not agree with the remaining experimental data. This observation can also be made for the experimen-

tal value of D_{12}^{M} at state point #4, which should be higher as predicted by molecular simulation. As mentioned in the discussion of the experimental results, these problems are due to the poor optical properties in that composition region.

The comparison of the eigenvalues of the Fick diffusion matrix between simulation and experiment is shown in Fig. 11 along paths A and B, respectively. As expected from the favorable agreement of the elements of the diffusion matrix, there is a very good qualitative and quantitative agreement between predictions from simulation and experimental data with an overall mean absolute average deviation of 7% and 9% for the first and second eigenvalues, respectively. Along path A, the first eigenvalue is underestimated by molecular simulation and the second eigenvalue agrees, in general, within uncertainty with the experimental results. Along path B, the agreement of both eigenvalues is excellent, with the exception of the the second eigenvalue at state point #2. However, as can be seen in Fig. 11, the experimental value at this state point does not correspond well with the remaining experimental data.

Conclusions

This is one of the first, if not the very first, coordinated experimental and molecular simulation effort to study diffusion in ternary liquid mixtures. The systematic and quantitative examination of the Fick diffusion coefficients of the mixture water + methanol + ethanol at 298.15 K and 0.1 MPa was performed experimentally by the Taylor dispersion technique and by molecular simulation. In a parallel effort, the four Fick diffusion coefficients of the ternary mixture were measured and computed along two concentration paths starting at one binary subsystem and moving towards another one, *i.e*, w_1 = 0.1 kg kg^{-1} (path A) or w_2 = 0.44 kg kg^{-1} (path B) was held constant. Furthermore, the validity of the Onsager reciprocal relations was tested for all measured state points, coming to the conclusion that they are valid within an acceptable range of error.

On the whole, the reproducibility of the experimental results was excellent in terms of the pseudo-binary diffusion coefficients and the Taylor peak shapes. The fitting of the experimental

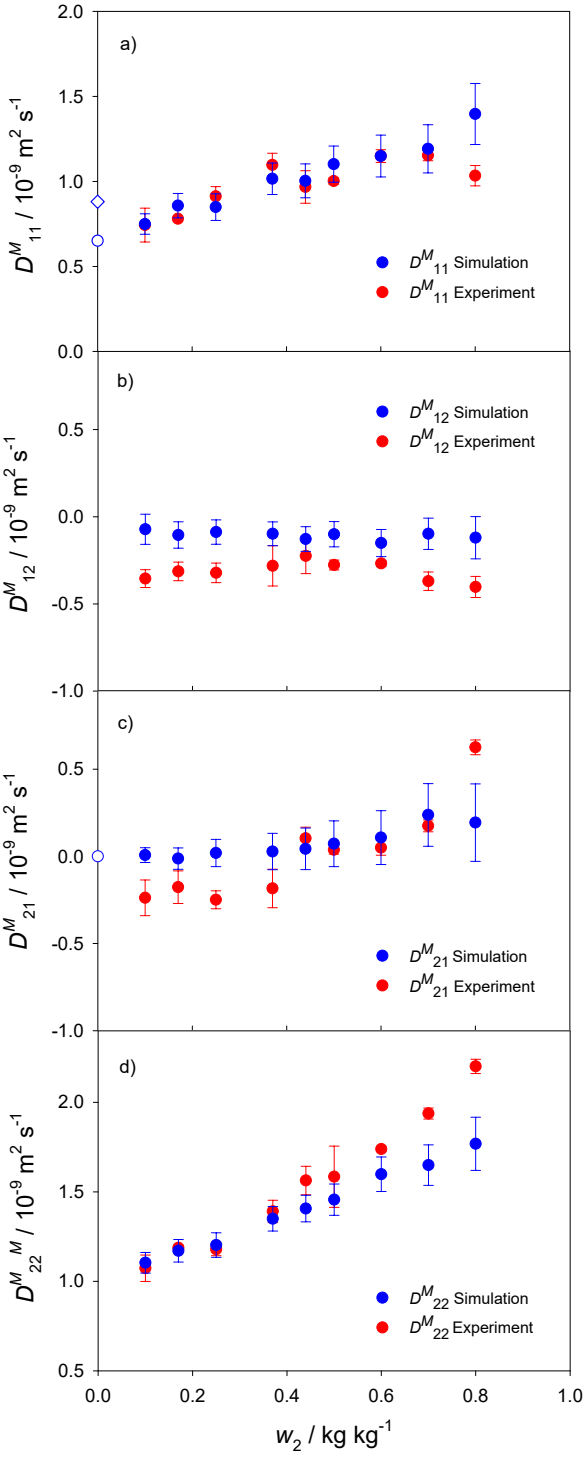

Figure 9: Simulation results of the Fick diffusion coefficients (a) D^M_{11}, (b) D^M_{12}, (c) D^M_{21} and (d) D^M_{22} along path A in the mixture water (1) + methanol (2) + ethanol (3) compared with present experimental results in the molar-averaged frame of reference. The empty symbols indicate asymptotic values approaching the binary subsystem.

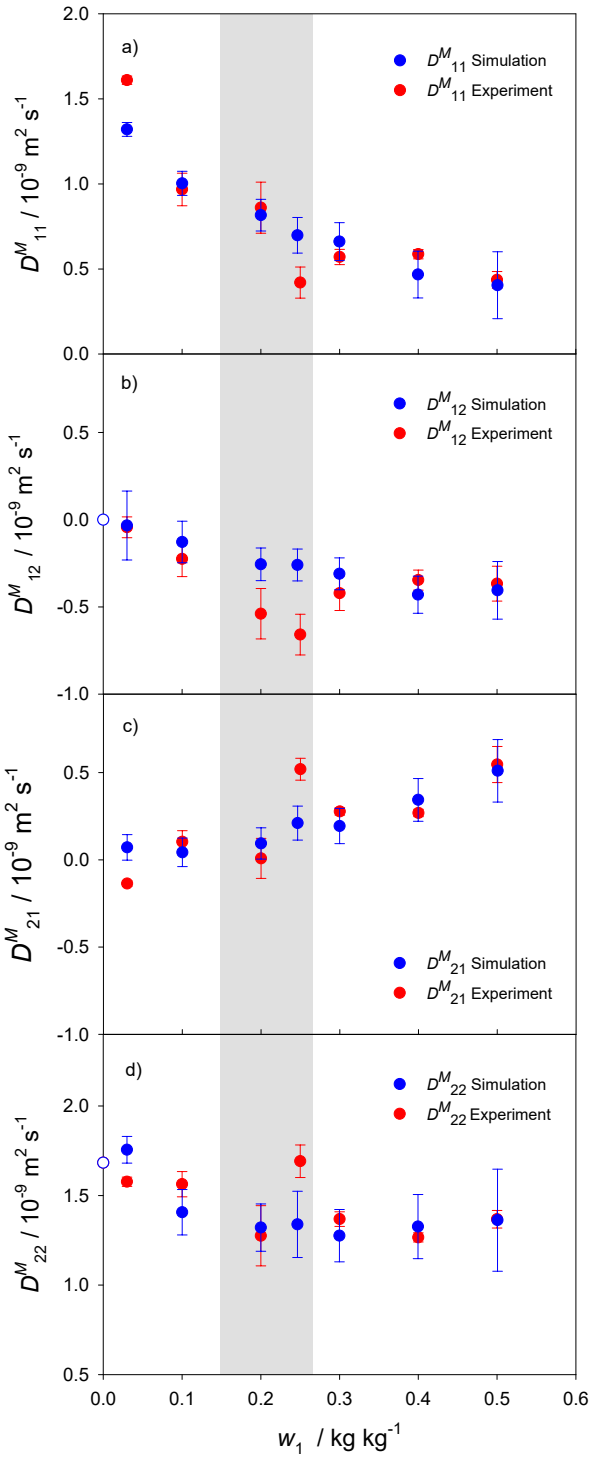

Figure 10: Simulation results of the Fick diffusion coefficients (a) D^M_{11}, (b) D^M_{12}, (c) D^M_{21} and (d) D^M_{22} along path B in the mixture water (1) + methanol (2) + ethanol (3) compared with present experimental results in the molar-averaged frame of reference. The empty symbols indicate asymptotic values approaching the binary subsystem. Poor optical properties were encountered in the shaded composition range.

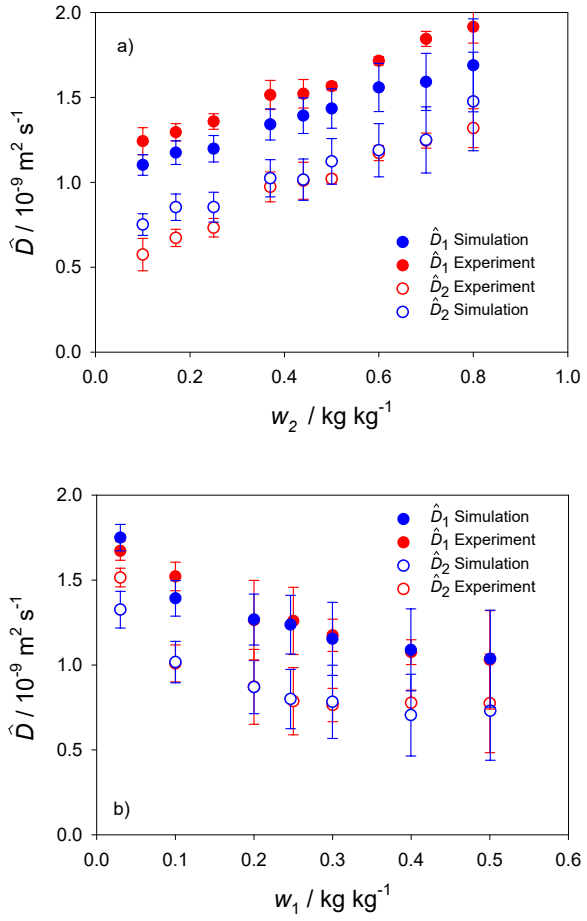

Figure 11: Simulation results of the the first and second eigenvalues of the Fick diffusion matrix along (a) path A and (b) path B in the mixture water (1) + methanol (2) + ethanol (3) compared with present experimental results.

data experienced difficulties for compositions which are very poor or rich in methanol content, *i.e.*, approaching binary limits on path A. While analyzing diffusion coefficients in the binary limit rich in methanol, along with strong scattering of the results on different days, we observed a Taylor peak with two maxima in the water-methanol subsystem, which identifies two different kinetics. Numerous studies at the molecular level[1–3] reported anomalous thermodynamic properties of alcohol-water mixtures. Our diffusion experiments on the macroscopic scale present evidence that a binary system may behave as a ternary one in methanol-rich mixtures.

Another feature of this mixture is the region with poor optical properties along a part of path B. This region is hard to sample experimentally and it gives priority to the simulations in terms of the reliability of the numerical coefficients values. This situation highlights the benefits of the simultaneous deployment of experiment and simulation.

Values for the MS diffusion coefficient matrix were sampled directly with EMD simulations and the Green-Kubo formalism, whereas the thermodynamic factor was obtained from MC simulations. The elements of the Fick diffusion matrix were calculated from those values. In order to compare the predicted simulation results and the experimental values, the experimental Fick diffusion coefficients were converted from the volume-averaged frame of reference to the molar-averaged frame of reference on the basis of experimental volumetric data from the literature. In general, a very good qualitative and quantitative agreement was obtained between molecular simulation predictions and experimental results for both main elements of the Fick diffusion matrix. The qualitative agreement of the cross elements of this matrix is also very good. As a result, both eigenvalues of the diffusion matrix are in an excellent overall agreement with each other.

It is expected that the molecular simulation methodology presented in this work can be employed to predict with similar accuracy also Fick diffusion coefficients at temperatures and pressures that are different from ambient conditions, which are experimentally more challenging.

The present EMD method yields the MS and intra-diffusion coefficients directly from one simulation run. Therefore, the simulation results for the intra-diffusion coefficients of all components in the mixture are given along both studied paths. The behavior of the intra-diffusion coefficients of

the mixture was analyzed in the light of its microscopic structure. The presence of clusters related to the unusually low value of the intra-diffusion coefficient for water at low water concentrations was observed, which corroborates the present experimental findings.

Appendix A. Simulation Details

All molecular simulations were carried out with the program *ms*2[54,55] in a cubic volume with periodic boundary conditions where the cut-off radius was set to $r_c = 17.5$ Å. Lennard-Jones long range interactions were considered using angle averaging[56]. Electrostatic long-range corrections were considered by the reaction field technique with conducting boundary conditions. The statistical uncertainties of the simulation data were estimated with a block averaging method.

In order to obtain the MS diffusion coefficients, EMD runs were performed in two steps: First, a simulation in the isobaric-isothermal (NpT) ensemble was carried out to calculate the density at the specified temperature, pressure and composition. In the second step, a canonic (NVT) ensemble simulation was performed at this temperature, density and composition to determine the time dependent auto-correlation functions. Newton's equations of motion were solved with a fifth-order Gear predictor-corrector numerical integrator. The temperature was controlled by velocity scaling. In all simulations, the integration time step was 0.99 fs. The simulations contained 5000 molecules, a number that according to our experience[6,14] is large enough to suppress finite size effects.

The simulations in the NpT ensemble were equilibrated over 3×10^5 time steps, followed by a production run over 5×10^6 time steps. In the NVT ensemble, the simulations were equilibrated over 3×10^5 time steps, followed by production runs of 5×10^7 time steps or about 50 ns. The auto-correlation functions were calculated using up to 2×10^5 independent time origins of the autocorrelation functions with a sampling length of 10 ps for all mixtures. That extensive length of the autocorrelation functions was chosen so that long-time tails corrections were not necessary. The separation between the time origins was chosen such that all autocorrelation functions have

decayed at least to $1/\mathrm{e}$ of their normalized value to achieve their time independence[57].

The simulation details and the corresponding equations for the determination of the thermodynamic factor are given in Ref.[6].

Appendix B. Numerical values of the partial molar volumes and G matrix

Table 8: Partial molar volumes $v_i/\mathrm{cm}^3\mathrm{mol}^{-1}$ for all components of the mixture water (1) + methanol (2) + ethanol (3) at 298.15 K and 0.1 MPa along path A ($w_1 = 0.1$ kg kg^{-1}) and path B ($w_2 = 0.44$ kg kg^{-1}).

Point #	x_1	x_2	x_3	v_1	v_2	v_3
			Path A			
11	0.213	0.120	0.667	15.56	40.51	58.47
12	0.208	0.199	0.593	15.51	40.54	58.48
13	0.202	0.284	0.514	15.45	40.56	58.49
14	0.194	0.404	0.402	15.38	40.58	58.50
15	0.186	0.523	0.291	15.33	40.60	58.48
16	0.180	0.608	0.212	15.30	40.62	58.46
17	0.175	0.688	0.137	15.29	40.63	58.42
18	0.170	0.764	0.066	15.29	40.65	58.38
			Path B			
2	0.062	0.510	0.428	14.55	40.73	58.62
3	0.190	0.469	0.341	15.35	40.60	58.49
4	0.340	0.421	0.239	16.09	40.32	58.27
5	0.404	0.400	0.196	16.39	40.18	58.08
6	0.462	0.381	0.157	16.68	40.01	57.82
7	0.563	0.349	0.088	17.18	39.59	57.12
8	0.649	0.321	0.030	17.58	39.07	56.31

Table 9: Elements of the symmetric Hessian matrix G for the mixture water (1) + methanol (2) + ethanol (3) at 298.15 K and 0.1 MPa along path A ($w_1 = 0.1$ kg kg^{-1}) and path B ($w_2 = 0.44$ kg kg^{-1}).

Point #	x_1	x_2	x_3	G_{11}/RT	$G_{12,21}/RT$	G_{22}/RT
			Path A			
11	0.213	0.120	0.667	4.443	0.806	9.911
12	0.208	0.199	0.593	4.731	0.993	6.779
13	0.202	0.284	0.514	5.106	1.253	5.518
14	0.194	0.404	0.402	5.807	1.783	4.999
15	0.186	0.523	0.291	6.919	2.715	5.364
16	0.180	0.608	0.212	8.325	3.985	6.369
17	0.175	0.688	0.137	11.014	6.540	8.739
18	0.170	0.764	0.066	18.858	14.254	16.318
			Path B			
2	0.062	0.510	0.428	16.812	1.685	4.333
3	0.190	0.469	0.341	6.341	2.220	5.088
4	0.340	0.421	0.239	4.950	3.352	6.544
5	0.404	0.400	0.196	5.233	4.205	7.563
6	0.462	0.381	0.157	6.011	5.028	8.932
7	0.563	0.349	0.088	10.145	10.165	14.047
8	0.649	0.321	0.030	30.890	31.416	35.670

Acknowledgement

The molecular simulation work was funded by the Deutsche Forschungsgemeinschaft (DFG) under the grant VR 6/11-1. The simulations were carried out on the national supercomputer Hazel Hen at the High Performance Computing Center Stuttgart (HLRS) within the project MMHBF2. The Brussels team is thankful to Dr. A. Mialdun (ULB) for fruitful discussions and to the PRODEX program of the Belgian Federal Science Policy Office and ESA for financial support.

References

(1) Dixit, S.; Crain, J.; Poon, W. C. K.; Finney, J. L.; Soper, A.K. Molecular segregation observed in a concentrated alcohol-water solution. *Nature* **2002**, *416*, 829.

(2) Bakó, I.; Megyes, T.; Bálint, S.; Grósz, T.; Chihaiab, V. Water-methanol mixtures: topology of hydrogen bonded network. *Phys. Chem. Chem. Phys.* **2008**, *10*, 5004–5011.

(3) Nedić, M.; Wassermann, T. N.; Larsen, R. W.; Suhm, M. A. A combined Raman- and infrared jet study of mixed methanol–water and ethanol–water clusters. *Phys. Chem. Chem. Phys.* **2011**, *13*, 14050–14063.

(4) Derlacki, Z. J.; Easteal, A. J.; Edge, A. V. J.; Woolf, L. A. Diffusion Coefficients of Methanol and Water and the Mutual Diffusion Coefficient in Methanol-Water Solutions at 278 and 298 K. *J. Phys. Chem.* **1985**, *89*, 5318–5322.

(5) van de Ven-Lucassen, I. M. J. J.; Kieviet, F. G.; Kerkhof, P. J. A. M. Fast and Convenient Implementation of the Taylor Dispersion Method. *J. Chem. Eng. Data* **1995**, *40*, 407–411.

(6) Pařez, S.; Guevara-Carrion, G.; Hasse H.; Vrabec, J. Mutual diffusion in the ternary mixture of water + methanol + ethanol and its binary subsystems. *Phys. Chem. Chem. Phys.* **2013**, *15*, 3985–4001.

(7) Dunlop, P. J.; Gosting, L. J. Interacting Flows in Liquid Diffusion: Expressions for the Solute Concentration Curves in Free Diffusion, and their Use in Interpreting Gouy Diffusiometer Data for Aqueous Three-component Systems. *J. Am. Chem. Soc.* **1955**, *77*, 5238–5249.

(8) Fick, A. E. Über Diffusion. *Pogg. Ann. Phys. Chem.* **1855**, *94*, 59–86.

(9) Vrentas, J. S.; Vrentas, C. M. Theoretical Aspects of Ternary Diffusion. *Ind. Eng. Chem. Res.* **2005**, *44*, 1112–1119.

(10) Maginn, E. J.; Elliot, J. R. Historical Perspective and Current Outlook for Molecular Dynamics as a Chemical Engineering Tool. *Ind. Eng. Chem. Res.* **2010**, *49*, 3059–3078.

(11) van Gunsteren, W. F.; Berendsen, H. J. C. Computer Simulation of Molecular Dynamics: Methodology, Applications, and Perspectives in Chemistry. *Angew. Chem.* **1990**, *129*, 992–1023.

(12) Liu, X.; Martín-Calvo, A.; McGarrity, E.; Schnell, S. K.; Calero, S.; Simon, J. M.; Bedeaux, D.; Kjelstrup, S.; Bardow, A.; Vlugt, T. J. H. Fick Diffusion Coefficients in Ternary Liquid Systems from Equilibrium Molecular Dynamics Simulations. *Ind. Eng. Chem. Res.* **2012**, *51*, 10247–10258.

(13) Liu, X.; Bardow, A.; Vlugt, T. J. H. Multicomponent Maxwell-Stefan Diffusivities at Infinite Dilution.*Ind. Eng. Chem. Res.* **2011**, *50*, 4776–4782.

(14) Guevara-Carrion, G.; Vrabec, J.; Hasse, H. Prediction of self-diffusion coefficient and shear viscosity of water and its binary mixtures with methanol and ethanol by molecular simulation. *J. Chem. Phys.* **2011**, *134*, 074508.

(15) Hawlicka, E.; Swiatla-Wojcik, D. Dynamic properties of the NaCl-methanol-water systems: MD simulation studies. *Phys. Chem. Chem. Phys.* **2000**, *2*, 3175–3180.

(16) van de Ven-Lucassen, I. M. J. J.; Vlugt, T. J. H.; van der Zanden, A. J. J.; Kerkhof, P. J. A. M. Molecular Dynamics Simulation of Self-Diffusion and Maxwell-Stefan Diffusion Coefficients in Liquid Mixtures of Methanol and Water. *Mol. Sim.* **1999**, *23*, 79–94.

(17) Wensink, E. J. W.; Hoffmann, A. C.; van Maaren, P. J.; van der Spoel, D. Dynamic properties of water/alcohol mixtures studied by computer simulation. *J. Chem. Phys.* **2003**, *119*, 7308–7317.

(18) Noskov, S. Y.; Lamoureux, G.; Roux, B. Molecular Dynamics Study of Hydration in Ethanol + Water Mixtures Using a Polarizable Force Field. *J. Phys. Chem. B* **2005**, *109*, 6705–6713.

(19) Zhang, C.; Yang, X. Molecular dynamics simulation of ethanol/water mixtures for structure and diffusion properties. *Fluid Phase Equilib.* **2005**, *231*, 1–10.

(20) Zhang, L.; Wang, Q.; Liu, Y.-C.; Zhang, L.-Z. On the mutual diffusion properties of ethanol-water mixtures. *J. Chem. Phys.* **2006**, *125*, 104502.

(21) Taylor, R.; Krishna, R. *Multicomponent Mass Transfer*; John Wiley & Sons: New York, 1993.

(22) Leaist, D. G. Relating multicomponent mutual diffusion and intradiffusion for associating solutes. Application to coupled diffusion in water-in-oil microemulsions. *Phys. Chem. Chem. Phys.* **2002**, *4*, 4732–4739.

(23) Price, W. E. Theory of the Taylor dispersion technique for three-component-system diffusion measurements. *J. Chem. Soc. Faraday Trans. 1* **1988**, *84*, 2431–2439.

(24) Walas, S. M. *Phase Equilibrium in Chemical Engineering*; Butterworths Publishers: Markham, 1985.

(25) Zarei, H. A.; Jalili, F.; Assadi, S. Temperature Dependence of the Volumetric Properties of Binary and Ternary Mixtures of Water (1) + Methanol (2) + Ethanol (3) at Ambient Pressure (81.5 kPa). *J. Chem. Eng. Data* **2007**, *52*, 2517–2526.

(26) Krishna, R.; van Baten, J. M. The Darken relation for multicomponent diffusion in liquid mixtures of linear alkanes: An investigation using molecular dynamics (MD) simulations. *Chem. Eng. Res.* **2005**, *44*, 6939–6947.

(27) Mills, R.; Malhotra, R.; Woolf, L. A.; Miller, D. G. Experimental Distinct Diffusion Data for 14 Binary Non-electrolyte Mixtures. *J. Chem. Eng. Data*, **1994**, *39*, 929–932.

(28) Taylor, R.; Kooijman, H. A. Composition Derivatives of Activity Coefficient Models for the Estimation of Thermodynamic Factors in Diffusion. *Chem. Eng. Comm.* **1991**, *102*, 87–106.

(29) Weerasinghe, S.; Smith, P. E. A Kirkwood-Buff Derived Force Field for Methanol and Aqueous Methanol Solutions. *J. Phys. Chem. B* **2005**, *109*, 15080–15086.

(30) Wedberg, R.; O'Connell, J. P.; Peters, G. H.; Abildskov, J. Pair correlation function integrals: computation and use. *J. Chem. Phys.* **2011**, *135*, 084113.

(31) Schnell, S. K.; Liu, X.; Simon, J. M.; Bardow, A.; Bedeaux, D.; Vlugt, T. J. H.; Kjelstrup, S. Calculating thermodynamic properties from fluctuations at small scales. *J. Phys. Chem. B* **2011**, *115*, 10911–10918.

(32) Keffer, D. J.; Adhangale, P. The composition dependence of self and transport diffusivities from molecular dynamics simulations. *Chem. Eng. J.*, **2004**, *100*, 51–69.

(33) Balaji, S. P.; Schnell, S. K.; McGarrity, E. S.; Vlugt, T. J. H. A direct method for calculating thermodynamic factors for liquid mixtures using the Permuted Widom test particle insertion method. *Mol. Phys.* **2012**, *111*, 287–296.

(34) Legros, J. C.; Gaponenko, Y.; Mialdun, A.; Triller, T.; Hammon, A.; Bauer, C.; Köhler, W.; Shevtsova, V. Investigation of Fickian diffusion in the ternary mixtures of water-ethanol-triethylene glycol and its binary pairs. *Phys. Chem. Chem. Phys.* **2015**, *17*, 27713.

(35) Mialdun, A.; Sechenyh, V.; Legros, J. C.; Ortiz de Zárate, J. M.; Shevtsova V. Investigation of Fickian diffusion in the ternary mixture of 1,2,3,4-tetrahydronaphthalene, isobutylbenzene, and dodecane. *J. Chem. Phys.* **2013**, *139*, 104903.

(36) Leahy-Dios, A.; Bou-Ali, M. M.; Platten, J. K.; Firoozabadi, A. Measurements of molecular and thermal diffusion coefficients in ternary mixtures. *J. Chem. Phys.* **2005**, *122*, 234502.

(37) Sechenyh, V.; Legros, J. C.; Mialdun, A.; Ortiz de Zárate, J. M.; Shevtsova, V. Fickian Diffusion in Ternary Mixtures Composed by 1,2,3,4-Tetrahydronaphthalene, Isobutylbenzene and n-Dodecane. *J. Phys. Chem. B* **2016**, *120*, 535–548.

(38) Königer, A., Wunderlich, H., Köhler, W. Measurement of Diffusion and Thermal Diffusion in Ternary Fluid Mixtures Using a Two-color Optical Beam Deflection Technique. *J. Chem. Phys.* **2010**, *132*, 174506.

(39) Larrañaga, M., Bou-Ali, M. M., Lizarraga, I., Madariaga, J. A., Santamaría, C. Soret Co-

efficients of the Ternary Mixture 1, 2, 3, 4-Tetrahydronaphthalene + Isobutylbenzene + n-Dodecane. *J. Chem. Phys.* **2015**, *143*, 024202.

(40) Leaist, D. G. Ternary diffusion coefficients of 18-crown-6 ether–KCl–water by direct least-squares analysis of Taylor dispersion measurements. *J. Chem. Soc. Faraday Trans.* **1991**, *87*, 597–601.

(41) van de Ven-Lucassen, I. M. J. J.; Kemmere, M. F.; Kerkhof, P. J. A. M. Complications in the Use of the Taylor Dispersion, Method for Ternary Diffusion Measurements: Methanol + Acetone + Water Mixtures. *J. Solution Chem.* **1997**, *26*, 1145–1167.

(42) Sechenyh, V. V.; Legros, J. C.; Shevtsova, V. Experimental and predicted refractive index properties in ternary mixtures of associated liquids. *J. Chem. Thermodynamics* **2011**, *43*, 1700–1707.

(43) Sechenyh, V. V.; Legros, J. C.; Shevtsova, V. Measurements of Optical Properties in Binary and Ternary Mixtures Containing Cyclohexane, Toluene, and Methanol. *J. Chem. Eng. Data* **2012**, *57*, 1036–1043.

(44) Sechenyh, V. V.; Legros, J. C.; Shevtsova, V. Optical properties of binary and ternary liquid mixtures containing tetralin, isobutylbenzene and dodecane. *J. Chem. Thermodynamics* **2013**, *62* 64–68.

(45) Ray, G. B.; Leaist, D. Measurement of Ternary Mutual Diffusion Coefficients from Ill-Conditioned Taylor Dispersion Profiles in Cases of Identical or Nearly Identical Eigenvalues of the Diffusion Coefficient Matrix. *J. Chem. Eng. Data* **2010**, *55*, 1814–1820.

(46) Schnabel, T.; Vrabec, J.; Hasse, H. Henry's law Constants of Methane, Nitrogen, Oxigen and Carbon dioxide in Ethanol from 273 to 498 K: Prediction from Molecular Simulation. *Fluid Phase Equilib.* **2005**, *233*, 134–143.

(47) Schnabel, T.; Srivastava, A.; Vrabec, J.; Hasse, H. Hydrogen bonding of methanol in supercritical CO2: Comparison between 1H-NMR spectroscopic data and molecular simulation results. *J. Phys. Chem. B* **2007**, *111*, 9871–9878.

(48) Abascal, J. L. F.; Vega, C. A general purpose model for the condensed phases of water: TIP4P/2005. *J. Chem. Phys.* **2005**, *123*, 234505.

(49) Königer, A.; Meier, B.; Köhler, W. Measurement of the Soret, diffusion, and thermal diffusion coefficients of three binary organic benchmark mixtures and of ethanol-water mixtures using a beam deflection technique. *Philos. Mag.* **2009**, *89*, 907.

(50) Miller, D. G. Thermodynamics of irreversible processes. The experimental verification of the Onsager reciprocal relations. *Chem. Rev.* **1960**, *60*, 15–37.

(51) Cussler, E. L. *Multicomponent Diffusion*; Elsevier: Amsterdam, 1976.

(52) Silva, C. M.; Liu, H.; Macedo, E. A. Models for self-diffusion coefficients of dense fluids, including hydrogen-bonding substances. *Chem. Eng. Sci.* **1998**, *53*, 2423–2429.

(53) Cibulka, I. Estimation of the excess volume and density of ternary liquid mixtures of non-electrolytes from binary data. *Collect. Czech. Commun.* **1982**, *47*, 1414–1419.

(54) Deublein, S.; Eckl, B.; Stoll, J.; Lishchuk, S.; Guevara-Carrion, G.; Glass, C. W.; Merker, T.; Bernreuther, M.; Hasse, H.; Vrabec, J. ms2: A molecular simulation tool for thermodynamic properties. *Comput. Phys. Commun.* **2011**, *182*, 2350–2367.

(55) Glass, C. W.; Reiser, S.; Rutkai, G.; Deublein, S.; Köster, A.; Guevara-Carrion, G.; Wafai, A.; Horsch, M.; Bernreuther, M.; Windmann, T.; Hasse, H.; Vrabec, J. ms2: A molecular simulation tool for thermodynamic properties, new version release. *Comp. Phys. Commun.* **2014**, *185*, 3302–3306.

(56) Lustig, R. Angle-average for the powers of the distance between two separated vectors. *Mol. Phys.* **1988**, *65*, 175–179.

(57) Schoen, M.; Hoheisel, C. The mutual diffusion coefficient D_{12} in binary liquid model mixtures. Molecular dynamics calculations based on Lennard-Jones (12-6) potentials. *Mol. Phys.* **1984**, *52*, 33–56.

Graphical TOC Entry